






# Influence of experimental methods on the mechanical properties of silk fibers: A systematic literature review and future road map

Cite as: *Biophysics Rev.* **4**, 031301 (2023); doi: [10.1063/5.0155552](https://doi.org/10.1063/5.0155552)

Submitted: 21 April 2023 · Accepted: 20 June 2023 ·

Published Online: 17 July 2023



Gabriele Greco,<sup>1,2,a)</sup>  Benjamin Schmuck,<sup>1,3</sup>  S. K. Jalali,<sup>2</sup>  Nicola M. Pugno,<sup>2,4</sup>  and Anna Rising<sup>1,3,a)</sup> 

## AFFILIATIONS

<sup>1</sup>Department of Anatomy, Physiology and Biochemistry, Swedish University of Agricultural Sciences, 75007 Uppsala, Sweden

<sup>2</sup>Laboratory for Bioinspired, Bionic, Nano, Meta, Materials & Mechanics, Department of Civil, Environmental and Mechanical Engineering, University of Trento, Via Mesiano, 77, 38123 Trento, Italy

<sup>3</sup>Department of Biosciences and Nutrition, Karolinska Institutet, Neo, 14186 Huddinge, Sweden

<sup>4</sup>School of Engineering and Materials Science, Queen Mary University of London, Mile End Road, London E14NS, United Kingdom

<sup>a)</sup>Authors to whom correspondence should be addressed: [gabriele.greco@slu.se](mailto:gabriele.greco@slu.se) and [anna.rising@ki.se](mailto:anna.rising@ki.se)

## ABSTRACT

Spider silk fibers are of scientific and industrial interest because of their extraordinary mechanical properties. These properties are normally determined by tensile tests, but the values obtained are dependent on the morphology of the fibers, the test conditions, and the methods by which stress and strain are calculated. Because of this, results from many studies are not directly comparable, which has led to widespread misconceptions in the field. Here, we critically review most of the reports from the past 50 years on spider silk mechanical performance and use artificial spider silk and native silks as models to highlight the effect that different experimental setups have on the fibers' mechanical properties. The results clearly illustrate the importance of carefully evaluating the tensile test methods when comparing the results from different studies. Finally, we suggest a protocol for how to perform tensile tests on silk and biobased fibers.

Published under an exclusive license by AIP Publishing. <https://doi.org/10.1063/5.0155552>

## TABLE OF CONTENTS

INTRODUCTION . . . . .	1
DETERMINATION OF THE DIAMETER . . . . .	2
STRAIN RATE . . . . .	4
COLLECTING SPEED . . . . .	4
HUMIDITY AND AGING . . . . .	5
FIBER MORPHOLOGY . . . . .	5
METHOD FOR CALCULATING STRESS AND STRAIN . . . . .	15
CONCLUSIONS . . . . .	17
MATERIALS AND METHODS . . . . .	18
Spinning artificial spider silk . . . . .	18
Native major ampullate silk . . . . .	18
Degummed <i>B. mori</i> silk . . . . .	18
Tensile tests . . . . .	18
Light microscopy . . . . .	18
Scanning electron microscopy . . . . .	18
Statistical analysis . . . . .	18
Simulations . . . . .	18

SUPPLEMENTARY MATERIAL . . . . .	18
----------------------------------	----

## INTRODUCTION

Natural load-bearing materials are often hierarchically structured and have excellent mechanical performance,<sup>1,2</sup> and silk fibers are of particular interest in this regard. Indeed, because of their mechanical and biological properties, they have already been used by ancient civilizations during the past thousands of years for textiles<sup>3–8</sup> or, e.g., as sutures.<sup>7,9,10</sup> In terms of toughness (ability to absorb energy before fracture), spider silk is a top-ranked biological material because of its strength and deformability [Fig. 1(a)].<sup>11,12</sup> Since silk fibers also are biodegradable and biocompatible,<sup>13</sup> they have been proposed to be useful for applications in the fields of biomedicine,<sup>9,10</sup> robotics,<sup>14</sup> and aerospace engineering.<sup>15</sup> For any large-scale industrial use of spider silk, methods to produce the fibers without using spiders must be developed. In line with this, over recent decades, the development of production and spinning methods for recombinant spider silk proteins

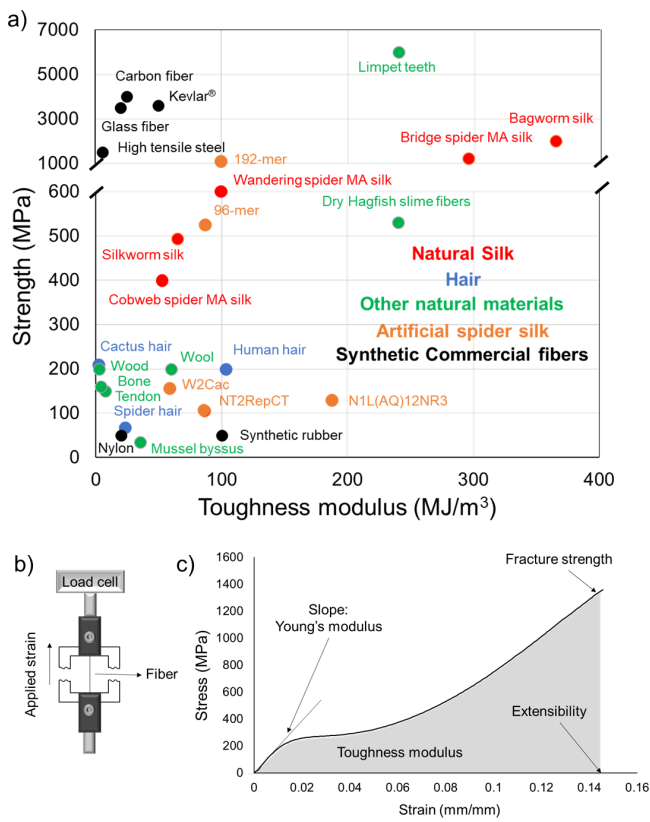


**FIG. 1.** (a) Ashby plot of a selection of natural and artificial fibers. Data obtained from the following references: natural silk<sup>16–20</sup> (this work for bridge spider, *Larinioides sclopetarius*), hair,<sup>21–23</sup> other natural materials,<sup>24–29</sup> artificial spider silk<sup>30–32</sup> (this work for NT2RepCT), and synthetic commercial fibers.<sup>27,33–35</sup> MA stands for Major Ampullate. These data represent the results from engineering stress and strain curves. (b) Typical setup to perform a tensile test on a silk fiber. The fiber is mounted on a frame that is clamped by two grips. One grip moves, applying a strain, and the elastic response (force) is measured by a load cell connected to one of the grips. The obtained raw data are load and displacement, which are converted into stress and strain. (c) Typical stress–strain graph for a spider silk fiber in which the main mechanical properties commonly reported in the silk field are highlighted. The Young's modulus is the slope of the linear fit in the first elastic region before the yield point. The toughness modulus is the area under the stress–strain curve. The extension at break, or extensibility is the ultimate strain value before fiber fracture, and the fracture strength is the maximal (here last) stress point before the fracture.

have been the main focus areas in the materials science field. Since the mechanical properties of the pristine fibers are one of the most attractive features of the material, and since these properties are sought in artificial replicas, reported values must be comparable between different studies.

To determine the mechanical properties of natural and artificial silk fibers, a static tensile test analyzer is commonly used. The fiber is placed in the instrument that applies a strain and records the elastic response of the fiber through a load cell [Fig. 1(b)]. In this way, a load–displacement curve is obtained, which is converted into a stress–strain curve [Fig. 1(c)]. To calculate the stress ( $\sigma$ ) that is applied to the fiber, the recorded force ( $F$ ) is divided by the cross-sectional area ( $A$ ),

$$\sigma = \frac{F}{A}. \quad (1)$$

The strain ( $\epsilon$ ) is the measure of the relative deformation and is obtained by the following equation:

$$\epsilon = \frac{\Delta L}{L}, \quad (2)$$

where  $\Delta L$  is the fiber elongation, and  $L$  is the gauge length of the fiber sample.

From the stress–strain curve, the following parameters can be extracted: (1) the fracture strength, i.e., the maximal stress that the material is able to sustain before fracture; (2) the extensibility, i.e., the maximal strain (or strain at break) of the material at fracture; (3) the Young's modulus, i.e., the initial slope of the stress–strain curve; and (4) the toughness modulus, i.e., the energy per unit of volume that the material absorbs before fracture, calculated as the area under the stress–strain curve.

Today's tensile test instruments are easily operated and very precise, but several factors need to be considered when comparing the mechanical properties of different materials, including the extrusion speed, collecting speed, and strain rate, as well as choice of methods for determining fiber diameter and for calculating of the mechanical properties. These parameters may appear as minor differences in the experimental protocols, but as we will show in the following paragraphs, they have a profound impact on fiber mechanics. On the other hand, if the field has reached a consensus on which methodological approach to use, the choice of method would be less important since all results would be obtained in the same manner and thereby comparable. A survey of the literature on silk fiber mechanics, however, shows that the field is far from uniform, and strikingly, in many cases, experimental details are not even reported (Fig. 2, Fig. S1, supplementary material Sec. S1). Below we address each of these parameters one by one and illustrate their respective impact on the fibers' mechanical properties using both published and original data. Finally, we propose guidelines in the design of tensile tests and list critical aspects for assessing the validity of reported silk fiber mechanical properties.

## DETERMINATION OF THE DIAMETER

An important source of error in calculating the mechanical properties of silk fibers is the measurement of the fiber diameter, which is used for calculating the cross-sectional area and the stress defined in Eq. (1). This may seem like a simple task, but as described below, it can be difficult to do in a precise manner, and the choice of method will substantially impact the obtained stress values. For silk fibers with a circular cross section, the dimension of the diameter is obtained with either light microscopy (LM) or Scanning Electron Microscopy (SEM) [Fig. 2(c)]. Both techniques have advantages and disadvantages with respect to ease of use, resolution, and risk of artifacts.

Light microscopy allows a fairly accurate measure of micrometric dimensions by using visible light,<sup>36</sup> but it is limited by the resolution for a specific wavelength ( $\lambda$ ), as described by the Abbe diffraction limit

$$\text{resolution} \cong \frac{\lambda}{2.8}.$$

Thus, objects that in one or several dimensions are smaller than around  $0.25 \mu\text{m}$  cannot be accurately measured by light microscopy.<sup>37</sup> Most major ampullate silk fibers have a diameter between 3 and

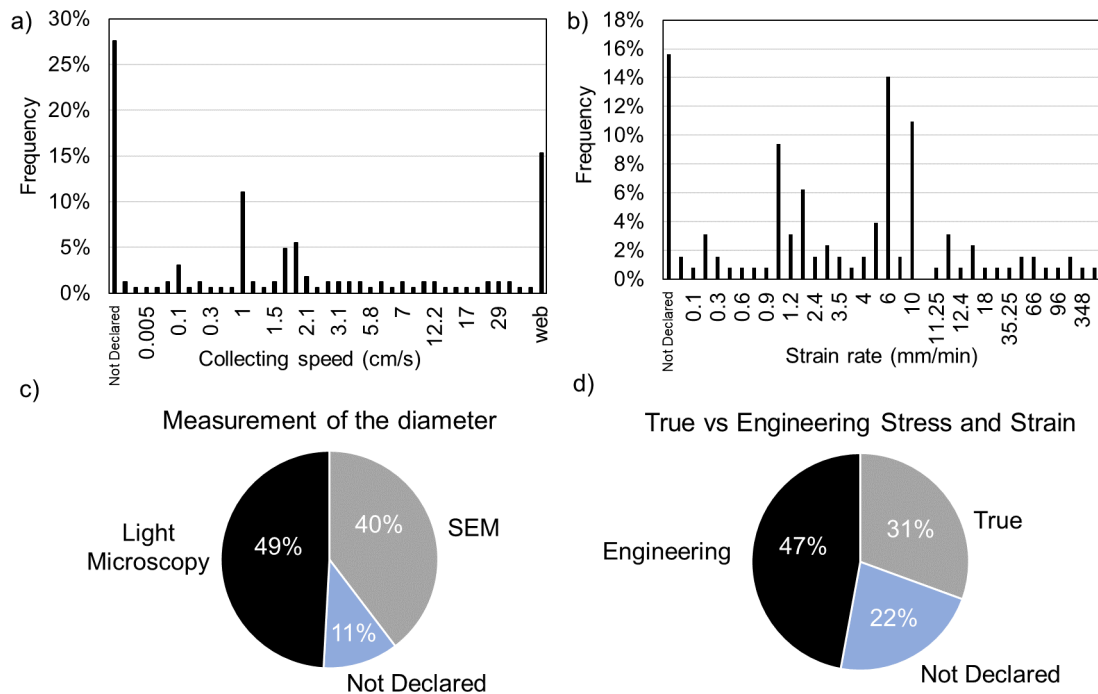


**FIG. 2.** Fraction of studies in which the mechanical properties have been obtained using (a) different collecting fibers speed (“web” means that the fibers were collected either from the web or the natural strands spun by the spiders obtained without forced silking), (b) tensile testing at different strain rates, and (c) light microscopy or scanning electron microscopy (SEM) to determine the diameter. Panel (d) illustrates the fraction of studies reporting the mechanical properties of silk fibers using engineering stress and strain, true stress and true strain, or not declared, respectively.

$6\ \mu\text{m}$ ,<sup>12,38</sup> which makes it possible to measure the diameter by light microscopy. On the other hand, natural spider silk spun by the spiders of the Mygalomorphae family<sup>39,40</sup> and silk spun from the aciniform and piriform glands<sup>41,42</sup> have diameters below  $1\ \mu\text{m}$  and are thus difficult to be accurately measured with this technique. However, an important advantage of light microscopy is that the sample does not require any pretreatment and that the technique is noninvasive, which implies that the observed sample can be recovered after the analysis without compromising its properties. Thereby, the average diameter for each fiber to be tensile tested can be obtained and then used when calculating the mechanical properties.

The other available technique to determine the diameter of silk fibers is SEM. With SEM, it is possible to obtain high-resolution images of details that under ideal conditions may reach nanometric dimensions.<sup>43</sup> During the measurement, the fiber is placed in a vacuum and must be pre-coated with conductive materials, both of which can lead to altered morphology of the fiber.<sup>44–48</sup> Furthermore, the experimental procedure makes it impossible to investigate the same fiber before the tensile testing, which is why the method only can be used to determine the average diameter of a particular fiber type.

The differences in diameters of silk fibers obtained by these two methods have been described by Blackledge *et al.*<sup>38</sup> who showed that using SEM will result in an underestimation of fiber diameter by about 10% compared to light microscopy. Considering that the diameter is used to calculate the circular cross-sectional area and that the area is the denominator in the stress calculation, using SEM for determining fiber dimensions may increase the calculated stress by up to 24%

compared to light microscopy. A comparison between SEM and light microscopy for obtaining artificial spider silk diameters has not been reported in the literature, but herein we show that the same differences are also found for NT2RepCT fibers (Fig. 3, Fig. S2). Despite that the method for determining the fiber diameter has such a large impact on the calculated tensile strength, the field has not settled on a common practice; 40% of studies reporting on silk fiber mechanical properties used SEM to evaluate the diameter, 49% used light microscopy, and

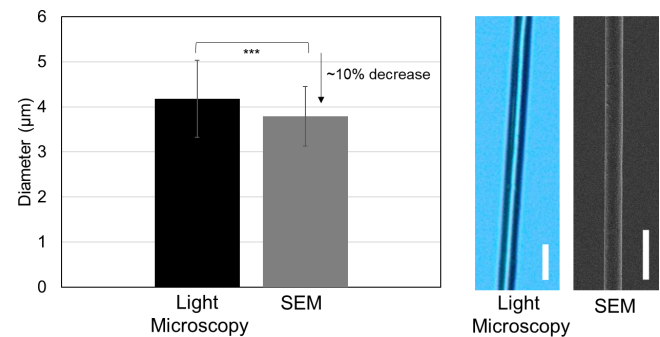


**FIG. 3.** The overall average and standard deviation of the diameters measured with the light microscopy (LM) and scanning electron microscopy (SEM) of  $n = 100$  NT2RepCT fibers, respectively. Representative light microscopy and SEM images of these fibers are shown on the right, where the scale bars are  $10\ \mu\text{m}$ . Stars indicate that the difference is significant ( $p < 0.0005$ ). The error bars are standard deviations.

the remaining 11% omitted this information [Fig. 2(c)]. Since the use of light microscopy makes it possible to determine the average diameter of individual fibers that subsequently can be tensile tested (thus taking into account fiber-to-fiber variability<sup>38</sup>) and since this piece of equipment is commonly available, we suggest that light microscopy should be used when determining the silk fiber diameter.

### STRAIN RATE

When comparing the mechanical properties of different fibers, it is important to consider how the test was performed, i.e., the instrument settings. Testing spider silk fibers at different strain rates will result in different mechanical properties because of their viscoelastic nature<sup>49–52</sup> [Fig. 2(b)]. The viscoelastic properties of silk are a result of the two-phase composition of the fiber in which tightly packed  $\beta$ -sheet crystals are embedded in a more amorphous matrix.<sup>53–56</sup>

The mechanical behavior of viscoelastic materials can in many cases be adequately approximated with the Kelvin–Voigt model,

$$\sigma = E\epsilon + \eta \frac{d\epsilon}{dt}, \quad (3)$$

in which  $E$  is the elastic modulus, and  $\eta$  is the viscosity of the material. The expression  $d\epsilon/dt$  is a measure of the strain rate, i.e., how fast the strain level of the material changes. From Eq. (3) it is thus clear that, given a specific viscosity, the faster the material is pulled, the faster the stress increases. This has been confirmed to hold true for spider major ampullate silk in the earliest studies on its mechanical properties. In the work of Denny,<sup>57</sup> the silk was tested at different strain rates of 1 up to 35 mm/min, which led to an increase in  $\sim 70\%$ ,  $\sim 200\%$ , and  $\sim 70\%$  in strength, Young's modulus, and toughness modulus, respectively. No significant changes were reported for the strain at break. These results were recently confirmed by Yazawa *et al.*,<sup>58</sup> who tested major ampullate silk fibers at strain rates between 0.01 and 1000 mm/min. The increase in the mechanical properties due to higher strain rates

was also confirmed by Cheng *et al.*,<sup>52</sup> in which the mechanical properties of *Araneus ventricosus* major ampullate silk were determined between 0.03 and 60 mm/min. In this range, the increase in the strength, Young's modulus, and toughness modulus were  $\sim 60\%$ ,  $\sim 60\%$ , and  $\sim 250\%$ , respectively. These results are also in agreement with our experiments performed on *Bombyx mori* silk (Fig. S3).

The dependence on the strain rate for artificial silk fibers has not been studied to a great extent, and it is plausible that the effect of different strain rates could differ between different artificial spider silk types, in line with what is observed for natural silks. Therefore, we tested NT2RepCT fibers at different strain rates and could detect a significant increase in the strength ( $\sim 100\%$ ) and Young's modulus ( $\sim 75\%$ ) when increasing the strain rate from 0.6 to 600 mm/min (Fig. 4). The strain at break initially increased when the strain rate was increased to 6 mm/min but decreased at higher values. Thus, using higher strain rates will apparently increase the values for stress and Young's modulus for NT2RepCT fibers, similar to what is observed for native silk.

The most commonly used strain rates are 1, 6, and 10 mm/min [Fig. 2(b)], which are within a range where there is little effect on the mechanical properties. Noticeable differences occur at strain rates higher than 10 mm/min and lower than 1 mm/min.<sup>52,57,58</sup> Still, Fig. 4 highlights the importance of explicitly declaring the strain rate, which in at least one experimental setup should be in the range 5–10 mm/min to be comparable to most scientific literature related to silk (Fig. 2) and other polymeric materials.<sup>29,59–62</sup> However, this should not be interpreted as a recommendation to avoid using higher strain rates as such settings would more closely reflect conditions that the fibers would experience in real world applications. Notably, the strain rate was not stated in 16% of the studies reviewed herein [Fig. 2(b)].

### COLLECTING SPEED

The mechanical properties of fibers made from the same feedstock (starting material) can vary since they are influenced by the

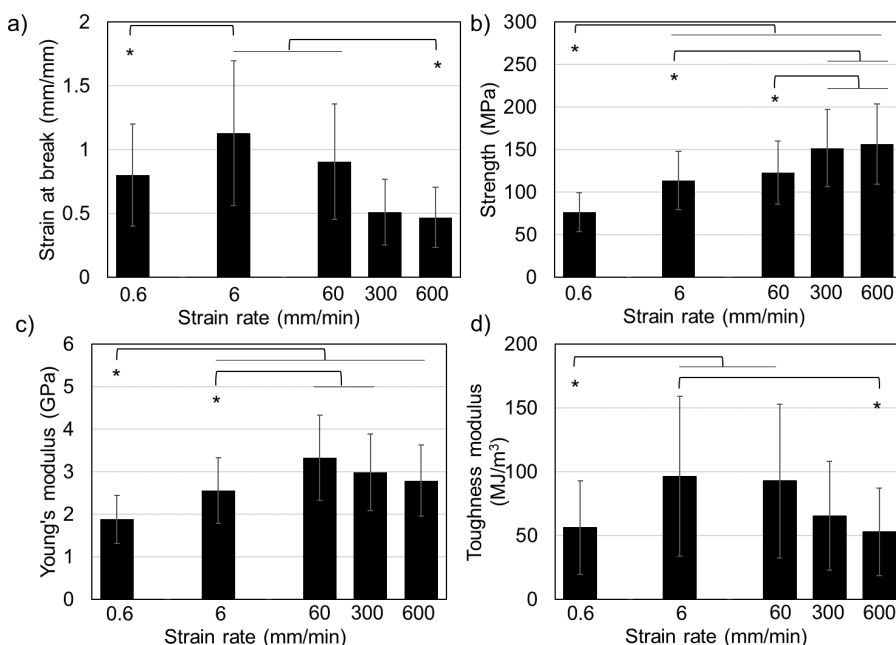


**FIG. 4.** Mechanical properties vs the strain rate at which the NT2RepCT fibers are tested: (a) strain at break, (b) strength, (c) Young's modulus, and (d) toughness modulus. Stars indicate that the difference is significant ( $p < 0.05$ ). The error bars are standard deviations.



extrusion and the collection process.<sup>59</sup> In particular, when spinning polymeric materials, it is expected that increased shear forces during fiber formation lead to an increased orientation of the polymer chains, positively affecting the tensile strength and Young's modulus of the spun fiber.<sup>63–65</sup> Collecting a polymeric fiber faster would in principle increase such shear forces. This is expected to be valid also for native silk, since it is a polymeric material, and some reports also align with this expectation.

Vollrath *et al.*<sup>66</sup> and Young *et al.*<sup>67</sup> presented data on silk collected between 0.01 and 12.8 cm/s from the species *Trichonephila edulis* and *Trichonephila senegalensis*, respectively, and showed that the fiber diameter and strain at break were reduced at increased collecting speeds, while Young's modulus and the strength increased with higher collecting speed until 2.5 cm/s, after which they decreased. However, a contradictory report was published by Cunnif *et al.*,<sup>68</sup> in which the silk of *Trichonephila clavipes* was collected at a speed ranging from 1.5 to 12.2 cm/s without significant changes in mechanical properties. In addition, Yazawa and coauthors studied the effect of collecting speed on both *Trichonephila clavata*<sup>69</sup> and different silkworms,<sup>70</sup> again concluding that the mechanical properties are not affected by this parameter. To further complicate the issue, higher collecting speed does not necessarily correspond to higher collecting stress, and both these parameters can affect the mechanical properties of the fibers.<sup>71,72</sup> Thus, more research is needed to understand the effects of collecting speed on the mechanical properties of natural silks.

When considering artificial spider silk, the effect of collecting speed on the fibers' mechanical properties is not easy to understand from the literature. This is due to that collecting speed is an imprecise parameter whose effects are influenced also by dope viscosity, extrusion speed, nozzle dimensions, and post-spin stretch, which differ in different spinning setups and are seldom fully reported in the literature [Table I, Fig. 2(a)]. However, Schmuck *et al.*<sup>73</sup> found that increased collecting speed in a system where all other parameters were kept constant indeed resulted in a significant stiffening and strengthening of artificial silk fibers, in line with what is known from synthetic fiber spinning. Consequently, despite the questionable value of considering collecting speed as such when comparing the mechanical properties of artificial silk fibers, we argue that it is important to report the collecting speed as precisely as possible (along with the other spinning parameters) to aid the assessment, comparison, and reproducibility of the data in the literature.

## HUMIDITY AND AGING

An important factor that must be considered when testing bio-based fibers is the relative humidity (RH). This is because water molecules that enter the fibers will break or weaken hydrogen bonds, which leads to structural reorganization and altered mechanical properties.<sup>74</sup> For native and artificial spider silk, testing fibers at RH higher than 70% (60% for recombinant spider silk) results in significantly lower values of Young's modulus and strength, but higher strain at break.<sup>75–78</sup> For artificial silk fibers, the sensitivity of the fibers to RH strongly depends on the amino acid residue sequence of the protein used to spin the fibers,<sup>12,77,79,80</sup> which is the reason why the tests should be done in dry conditions ( $15\% < \text{RH} < 50\%$ ) if the effects of the humidity are not known. The effects that humid conditions have on the structure and mechanical performance of the fiber are not

completely reversible, which makes it crucial to also consider the storage conditions of the fibers in the interim between spinning and tensile testing. Despite this, the RH is seldom considered, which is why we solicitate future studies to report the RH both during storage and tensile testing.

Another crucial aspect to consider when evaluating fiber mechanical properties is the aging process that the fibers will undergo. In polymer science, aging is a phenomenon for which the properties of a polymer change over time due to that the polymeric chain network is in a non-equilibrium thermodynamical state.<sup>81</sup> Because of this, the polymeric chains tend to change conformation toward a more stable thermodynamical state over time,<sup>82</sup> which results in altered properties of the material.<sup>83</sup> Unfortunately, the changes in the properties strongly depend on the polymer type,<sup>84</sup> and aging effects must therefore be studied individually for each polymer fiber type. Aging of natural and artificial silk fiber has been notoriously ignored, but a single report shows that over time, native spider silk undergoes an increase in Young's modulus and a decrease in strain at break.<sup>85</sup> For these reasons, it is important that the time between spinning and tensile testing is reported, and, preferably, it should be kept constant in different experimental setups.

## FIBER MORPHOLOGY

Since the stress calculation is dependent upon the precise determination of the cross-sectional area, knowledge about the morphology of the fiber is crucial, but calculating the cross-sectional area of fibers with an imperfect cylindrical shape is challenging. The shape of commercially available fibers and natural silks fibers is consistent and homogeneous over the entire length of a fiber, even though they do not necessarily possess a round cross-section.<sup>16,86–88</sup> On the other hand, synthetic fibers produced for research purpose often suffer from major shape inhomogeneities.<sup>89–92</sup> This is valid also for artificial silk, but this aspect is seldom discussed when the mechanical properties are reported.<sup>30,32,77,93–108</sup> Since the cross-sectional area of such fibers is difficult to determine, the calculation of the tensile strength and toughness modulus is not precise.

When the shape of a silk fiber cross-section deviates from a circle, the commonly accepted procedure to estimate the cross-sectional area is to measure the diameter at several randomly selected locations along the fiber's length and compute the average. The average diameter is then used to calculate the cross-sectional area assuming a circular shape. In doing so, the true cross-sectional area is likely to be overestimated, thereby underestimating the stress and other properties that depend on it (strength, Young's modulus, and toughness modulus).<sup>103</sup> To illustrate how drastically the computed mechanical properties can differ when the cross-sectional area is not carefully determined, we used NT2RepCT fibers that harbored a longitudinal groove alternating with a roundish cross section [Fig. 5(a), Fig. S4] which is a shape also commonly reported for other artificial silk fibers.<sup>77,89,93,94,100–102,108–110</sup> As depicted in Figs. S5(a) and S5(b), a circle with the same "diameter" as a fiber exhibiting a longitudinal groove would have a larger estimated cross-sectional area. In the case of NT2RepCT fibers, measuring the "diameter" when observing the face of a fiber with the longitudinal groove means that the true cross-sectional area is overestimated by a factor of  $\sim 1.81$  [Figs. S5(c)–S5(e)], if a circular cross-section is assumed.

**TABLE I.** The mechanical properties of natural and artificial spider silk and the experimental setup used. LM=fiber diameter measured with light microscopy; E=Engineering stress and strain; SEM=diameter measured with scanning electron microscopy; T=True stress and true strain. ND means that it was not either declared which method that was used to calculate the stress and strain.

Reference	Year	Spider species	Silk collection speed (cm/s)	Diameter	Diameter measured prior or after fracture?	Cross-section evaluation	Gauge length (mm)	Strain rate (mm/min)	True or Eng. Stress-strain curve
Wilson <sup>121</sup>	1962	<i>Araneus diadematus</i>	18	LM	Prior dry and silk stained in shirlastain A (I.C.I.) and mounted in de Faure's aqueous medium.	Circle	...	...	E
Denny <sup>57</sup>	1976	<i>L. scolopetarius</i>	Web	LM	Prior	Circle	25	0.75 3.5 35.25	T
Work <sup>122</sup>	1976	<i>Trichonephila madagascariensis</i> ; <i>A. diadematus</i> ; <i>Argiope aurantia</i> ; <i>Argiope argentata</i> ; <i>Eriophora fuliginea</i>	Web; forcibly extracted (anaesthetized and silked with not declared speed)	LM	Prior	... (used textile units)	12.5	12.5	Units of textile measurement
Work <sup>49,123</sup>	1977, 1985	<i>L. scolopetarius</i> ; <i>A. diadematus</i> ; <i>Araneus gemma</i>	Web; Forcibly silked (spiders fell down) with not declared speed	LM	Prior	Circle	6.5–12.5	12.5	T
Gosline <i>et al.</i> <sup>124</sup>	1986	<i>L. scolopetarius</i>	Web	LM	Prior	Circle	25	3.5	T
Cunniff <i>et al.</i> <sup>68</sup>	1994	<i>T. clavipes</i>	1.1; 1.5; 3.1; 6.1; 12.2	SEM	ND	Circle	50.8	304.8	ND
Shao <i>et al.</i> <sup>125</sup>	1999	<i>A. diadematus</i>	2	SEM	ND	Circle	ND	50%–gauge length per min	ND
Shao and Vollrath <sup>126</sup>	1999	<i>A. diadematus</i> ; <i>T. edulis</i> ; <i>Latrodectus mactans</i> ; <i>Euprosthenops sp.</i>	2	SEM	ND	Circle	7	50%–gauge length per min	ND
Madsen <i>et al.</i> <sup>127</sup>	1999	<i>Euprosthenops sp.</i> ; <i>Cyrtophora citricola</i> ; <i>L. mactans</i> ; <i>A. diadematus</i> ; <i>T. edulis</i>	ND; 0.4; 1; 2; 8; 10	SEM	ND	Circle	6.9	3	E
Pérez-Rigueiro <i>et al.</i> <sup>128</sup>	2001	<i>Argiope trifasciata</i>	From web	SEM	After	Circle	20	0.24	T
Vollrath <i>et al.</i> <sup>66</sup>	2001	<i>A. diadematus</i> ; <i>T. edulis</i>	0.005 – 95.0	SEM	ND	Circle	12	6	E
Lazaris <i>et al.</i> <sup>129</sup>	2002	<i>Araneus sp.</i> ; Artificial	ND	LM	Prior	Circle	~10	ND	ND

TABLE I. (Continued.)

Reference	Year	Spider species	Silk collection speed (cm/s)	Diameter	Diameter measured prior or after fracture?	Cross-section evaluation	Gauge length (mm)	Strain rate (mm/min)	True or Eng. Stress-strain curve
Guinea <i>et al.</i> <sup>130</sup>	2003	<i>A. trifasciata</i>	1	SEM	ND	Circle	20	1	T
Ko and Jovicic <sup>131</sup>	2004	<i>T. clavipes</i>	as Cunnif <i>et al.</i> <sup>68</sup>	ND	ND	Not declared	12.5	12.5	ND
Blackledge <i>et al.</i> <sup>38</sup>	2005	<i>A. trifasciata</i> ; <i>A. argentata</i> ; <i>Oloborus diversus</i> ; <i>Gasteracantha cancriformis</i> ; <i>Latrodectus hesperus</i> ; <i>G. cancriformis</i> ; <i>Peucetia viridans</i> ; <i>L. hesperus</i> ; <i>Araneus gemmoides</i>	Not declared, but declared to be obtained during prey attack, directly from webs, through forcible silking of restrained spiders, and from egg sacs.	LM; SEM	Prior	Circle	ND	1% of the gauge length per s	E
Blackledge <i>et al.</i> <sup>50</sup>	2005	<i>L. hesperus</i>	From web and forcibly extracted as explained in Work <sup>122</sup>	LM	Prior	Circle	21	1% of the gauge length per s	T
Guinea <sup>132</sup>	2005	<i>A. trifasciata</i>	1	SEM	Not declared	Circle	20	0.24	E
Liu <i>et al.</i> <sup>75</sup>	2005	<i>T. edulis</i>	0.2; 1; 2; 10; 20	SEM	Not declared	Circle	ND	ND	E
Ruigeiro <i>et al.</i> <sup>72</sup>	2005	<i>A. trifasciata</i>	0.1; 1	SEM	Not declared	Circle	20	0.24	E
Yang <i>et al.</i> <sup>133</sup>	2005	<i>T. edulis</i>	2	SEM	After	Measured surface area with SEM	10	3.6	ND
Blackledge and Hayashi <sup>134</sup>	2006	<i>A. argentata</i>	From web and forcibly extracted as explained in Work <sup>122</sup>	LM	Prior	Circle	21; 10	1%-gauge length per s	T
Swanson <i>et al.</i> <sup>135</sup>	2006	<i>T. clavipes</i> ; <i>A. argentata</i> ; <i>A. gemmoides</i> ; <i>L. hesperus</i> ; <i>Leucauge venusta</i> ; <i>Kukulcania hibernalis</i> ; <i>Plectreuryx tristis</i>	From web and forcibly extracted as explained in Work <sup>122</sup>	LM	Prior	Circle	ND	1%-gauge length per s	T; E
Guinea <i>et al.</i> <sup>115</sup>	2006	<i>A. trifasciata</i>	2	SEM	Prior and after (not clear)	Circle	25	1	T; E
Pérez-Rigueiro <i>et al.</i> <sup>136</sup>	2007	<i>A. trifasciata</i>	2	SEM	Prior (not clear)	Circle	20	0.24	T

TABLE I. (Continued.)

Reference	Year	Spider species	Silk collection speed (cm/s)	Diameter	Diameter measured prior or after fracture?	Cross-section evaluation	Gauge length (mm)	Strain rate (mm/min)	True or Eng. Stress-strain curve
Agnarsson <i>et al.</i> <sup>137</sup>	2008	<i>A. gemmoides</i> ; <i>Parasteatoda tepidariorum</i> ; <i>A. argentata</i> ; <i>A. trifasciata</i> ; <i>Deinopis spinosa</i> ; <i>G. cancriformis</i> ; <i>Latrodectus geometricus</i> ; <i>L. hesperus</i> ; <i>Mastophora hutchinsoni</i> ; <i>Mastophora phrynosoma</i> ; <i>P. viridans</i> ;	From web and forcibly extracted as explained in Work <sup>122</sup>	LM	Prior	Circle	20.7	12.4	T
Savage and Gosline <sup>138</sup>	2008	<i>T. clavipes</i> ; <i>A. diadematus</i>	From dragline spun by the walking spider	LM	Prior	Circle	50	10	E
Ortlepp and Gosline <sup>139</sup>	2008	<i>Salticus scenicus</i> ; <i>A. diadematus</i>	From dragline spun by the walking spider	LM	Prior	Circle	60	20	ND
Lee <i>et al.</i> <sup>140</sup>	2009	<i>Areneus sp.</i>	1	LM	Prior	Circle	4	2	E
Sensenig <i>et al.</i> <sup>141</sup>	2010	<i>A. diadematus</i> ; <i>A. marmoreus</i> ; <i>A. trifolium</i> ; <i>A. aurantia</i> ; <i>A. trifasciata</i> ; <i>Caerostris darwini</i> ; <i>Cyclosa conica</i> ; <i>Eustala sp.</i> ; <i>G. cancriformis</i> ; <i>Larinioides cornutus</i> ; <i>L. venusta</i> ; <i>Mangora gibberosa</i> ; <i>Metepeira labyrinthea</i> ; <i>Micrathena gracilis</i> ; <i>Neoscona arabesca</i> ; <i>N. crucifera</i> ; <i>N. domiciliorum</i> ; <i>T. clavipes</i> ; <i>Nuctenea umbratica</i> ; <i>Tetragnatha versicolor</i> ; <i>Verrucosa arenata</i> ; <i>Zygiella x-notata</i>	From web	LM	Prior	Geometrical average of the diameter $d_h = 2\sqrt{2r_{ss}}$	11–16	66–96	T



TABLE I. (Continued.)

Reference	Year	Spider species	Silk collection speed (cm/s)	Diameter	Diameter measured prior or after fracture?	Cross-section evaluation	Gauge length (mm)	Strain rate (mm/min)	True or Eng. Stress-strain curve
Agnarsson <i>et al.</i> <sup>11</sup>	2010	<i>C. darwini</i>	From the web and forcibly as described in Pérez-Rigueiro <i>et al.</i> <sup>128</sup>	LM	Prior	Circle	16	96	T
Guinea <i>et al.</i> <sup>142</sup>	2010	<i>A. trifasciata</i>	Web	SEM	Prior (not clear)	Circle	5–9	1	T
Sensenig <i>et al.</i> <sup>143</sup>	2011	<i>N. arabesca</i>	Web	SEM	Prior	Geometrical average of the diameter $d_h = 2\sqrt{2r_{ss}}$	11–16	66–96	T
Pogozelski <i>et al.</i> <sup>144</sup>	2011	<i>Steatoda triangulosa</i>	Web	SEM	Not declared	Circle	25–26	12	ND
Hudspeth <i>et al.</i> <sup>145</sup>	2012	<i>T. clavipes</i>	20	SEM	Not declared	Circle	5–3	0.3–306 (high speed)	ND
Guinea <i>et al.</i> <sup>119</sup>	2012	<i>A. trifasciata</i> ; <i>Trichonephila inaurata</i>	ND	SEM	After	Circle	20	1	T
Blamires <i>et al.</i> <sup>146</sup>	2012	<i>Argiope aethereal</i> ; <i>A. aemula</i> ; <i>Cyclosa mulmeinensis</i> , <i>C. confuse</i> ; <i>Cyrtophora unicolor</i> ; <i>C. moluccensis</i> ; <i>Leucauge blanda</i> ; <i>L. tessellata</i> ; <i>Trichonephila clavata</i> ; <i>Trichonephila pilipes</i> .	1.7	LM	Prior	Circle	20	12	T
Blackledge <i>et al.</i> <sup>147</sup>	2012	<i>Aphonopelma seemanni</i> ; <i>K. hibernalis</i> ; <i>Scytodes sp.</i> ; <i>Phidippus regius</i> ; <i>P. viridans</i> ; <i>Tengella radiata</i> ; <i>Hogna heluo</i> ; <i>Dolomedes tenebrosus</i> ; <i>Pisaurina mirabilis</i> ; <i>D. spinosa</i> ; <i>Meta ovalis</i> ; <i>L. hesperus</i> ;	2	SEM	Prior	Circle	15	1.2	T

TABLE I. (Continued.)

Reference	Year	Spider species	Silk collection speed (cm/s)	Diameter	Diameter measured prior or after fracture?	Cross-section evaluation	Gauge length (mm)	Strain rate (mm/min)	True or Eng. Stress-strain curve
Blamires <i>et al.</i> <sup>148</sup>	2012	<i>C. darwini</i> ; <i>A. diadematus</i> ; <i>Argiope lobata</i> ; <i>A. trifasciata</i> ; <i>A. argentata</i> ; <i>A. aurantia</i> ; <i>A. bruennichi</i> ; <i>A. aethereal</i> ; <i>Cyrtophora moluccensis</i> ; <i>L. blanda</i>	1.7	LM	Prior	Circle	20	12	E
Steven <i>et al.</i> <sup>149</sup>	2013	<i>T. clavipes</i>	ND	LM	Prior	Circle	ND	2% (gauge length) min <sup>-1</sup>	ND
Porter <i>et al.</i> <sup>150</sup>	2013	<i>T. edulis</i>	ND	ND	Not declared	Not declared	ND	ND	ND
Marhabaie <i>et al.</i> <sup>151</sup>	2014	<i>A. trifasciata</i>	ND	LM	Prior	Circle	15.7	94.4	T
Xu <i>et al.</i> <sup>152</sup>	2014	<i>T. pilipes</i>	2.5	ND	Not declared	Not declared	20	10	ND
Heidebrecht <i>et al.</i> <sup>32</sup>	2015	<i>A. diadematus</i>	16.5 for native silk	LM	Prior	Circle	2	2.4	T
Blamires <i>et al.</i> <sup>153</sup>	2015	<i>T. pilipes</i>	1.7	LM	Prior	Circle	20	6	T
Perea <i>et al.</i> <sup>154</sup>	2015	<i>A. trifasciata</i> ; <i>T. inaurata</i>	0.1–1	SEM	Prior	Circle	20	1.2	T
Madurga <i>et al.</i> <sup>155</sup>	2016	<i>A. trifasciata</i> ; <i>A. aurantia</i> ; <i>A. lobata</i> ; <i>A. bruennichi</i> ; <i>A. diadematus</i> ; <i>C. darwini</i> ; <i>D. spinosa</i> ; <i>L. hesperus</i> ; <i>D. tenebrosus</i> ; <i>T. radiata</i> ; <i>P. regius</i>	ND	SEM	Prior	Circle	20	1.2	T
Lepore <i>et al.</i> <sup>85</sup>	2016	<i>L. cornutus</i>	Web	SEM	Prior	Circle	20	12	E
Benamù <i>et al.</i> <sup>156</sup>	2017	<i>Parawixia audax</i>	1.7	LM	Prior	Circle	10	6	T
Lepore <i>et al.</i> <sup>157</sup>	2017	<i>Holocnemus</i> sp.; <i>Pholcus</i> sp.; <i>Steatoda</i> sp.	Web	SEM	Prior	Circle	15	0.9	E
Koebley <i>et al.</i> <sup>158</sup>	2017	<i>Loxosceles laeta</i>	0.1–1	AFM	Not declared	...	5	1	ND
You <i>et al.</i> <sup>103</sup>	2018	Silkworms	Cocoon	LM	Prior	Circle	30	2	E

TABLE I. (Continued.)

Reference	Year	Spider species	Silk collection speed (cm/s)	Diameter	Diameter measured prior or after fracture?	Cross-section evaluation	Gauge length (mm)	Strain rate (mm/min)	True or Eng. Stress-strain curve
Xu <i>et al.</i> <sup>159</sup>	2018	(genetically modified to express major ampullate spidroin) Silkworms (genetically modified to express major ampullate spidroin)	Cocoon	SEM	Not declared	Circle	10	5	E
Kerr <i>et al.</i> <sup>160</sup>	2018	<i>T. pilipes</i> ; <i>Trichonephila plumipes</i>	Web	ND	Prior	Circle	ND	60	ND
Piorkowski <i>et al.</i> <sup>161</sup>	2018	<i>Hickmania troglodytes</i>	Web	LM	Prior	Circle	10	9	T
Blamires <i>et al.</i> <sup>162</sup>	2018	<i>Argiope keyserlingi</i> ; <i>Eriophora transmarina</i> ; <i>Latrodectus hasselti</i> ; <i>T. plumipes</i> ; <i>Phonognatha graeffei</i>	1.7	LM	Prior	Circle	10	6	T
Yazawa <i>et al.</i> <sup>163</sup>	2018	<i>T. clavata</i>	2.1	ND	Not declared	Not declared	5	10	E
Dellaquila <i>et al.</i> <sup>18</sup>	2019	<i>Cupiennius salei</i>	Web	LM	Prior	Circle	10	6	E
Viera <i>et al.</i> <sup>164</sup>	2019	<i>Badumna longinqua</i>	1.7	LM	Prior	Circle	10	6	T
Kong <i>et al.</i> <sup>88</sup>	2020	<i>T. pilipes</i>	ND	SEM	Not declared	Measured (cubic)	20	2	E
Pan <i>et al.</i> <sup>14</sup>	2020	<i>T. pilipes</i>	ND	SEM	Prior	Measured	ND	ND	ND
Garrote <i>et al.</i> <sup>165</sup>	2020	<i>Frigga crocuta</i> ; <i>Argyrodes elevatus</i> ; <i>Tetragnatha sp.</i> ; <i>Leucauge longimana</i> ; <i>Neoscona moreli</i> ; <i>G. cancriformis</i> ; <i>A. argentata</i>	Web; and forcibly silked as Work and Emerson <sup>166</sup> (~1 cm/s)	SEM	Prior	Circle	ND	1	T
Pantano <i>et al.</i> <sup>167</sup>	2020	<i>Meta menardi</i>	ND	ND	Not declared	Not declared	10	0.6	E
Wu <i>et al.</i> <sup>168</sup>	2020	<i>T. pilipes</i> ; Artificial silk	3–7; 1 (for artificial silk)	ND	Not declared	Not declared	ND	ND	ND

TABLE I. (Continued.)

Reference	Year	Spider species	Silk collection speed (cm/s)	Diameter	Diameter measured prior or after fracture?	Cross-section evaluation	Gauge length (mm)	Strain rate (mm/min)	True or Eng. Stress-strain curve
Kelly <i>et al.</i> <sup>169</sup>	2020	<i>T. pilipes</i>	1.7	LM	Prior	Circle	10	6	T
Greco and Pugno <sup>170</sup>	2020	<i>A. diadematus</i> ; <i>Ancylometes sp.</i> ; <i>Ceratogyrus marshalli</i> ; <i>C. salei</i> , <i>Grammostola rosea</i> ; <i>Linothele fallax</i> ; <i>N. umbratica</i> ; <i>Phoneutria fera</i> ; <i>Zygiella x-notata</i> .	1	LM	Prior	Circle	10	6	E
Yazawa <i>et al.</i> <sup>58</sup>	2020	<i>T. clavata</i>	2.1	SEM	Not clear	Circle	5	0.01–1000	E
Cheng <i>et al.</i> <sup>52</sup>	2020	<i>A. ventricosus</i>	Web	LM	Prior	Circle	20	0.3–60	E
Greco <i>et al.</i> <sup>171</sup>	2020	<i>C. salei</i>	1	LM	Prior	Circle	10	6	E
Hu <i>et al.</i> <sup>172</sup>	2020	<i>T. edulis</i>	2	SEM	Not declared	Circle	10	5	ND
Dugger <i>et al.</i> <sup>173</sup>	2020	<i>T. clavipes</i>	1	SEM	Prior	Circle	2	1.2	E
Htut <i>et al.</i> <sup>19</sup>	2021	<i>C. darwini</i> ; <i>A. trifasciata</i> ; <i>L. cornutus</i> ; <i>Parasteatoda tepidarium</i> ; <i>T. clavipes</i>	0.2; 6.5 (for <i>C. darwini</i> )	SEM	Not declared	Circle	12.58	11.25	T
Kono <i>et al.</i> <sup>120</sup>	2021	<i>C. darwini</i>	2.1	SEM	Prior	Circle	5	10	E
Yazawa and Sasaki <sup>69</sup>	2021	<i>T. clavata</i>	1–7	SEM	Prior	Circle	5	10	E
Greco and Pugno <sup>20</sup>	2021	<i>S. triangulosa</i> ; <i>S. paykulliana</i>	1	LM	Prior	Circle	10	6	E
Saric <i>et al.</i> <sup>174</sup>	2021	<i>A. diadematus</i>	1.2	LM	Prior	Circle	2	0.3	T
Piorkowski <i>et al.</i> <sup>175</sup>	2021	<i>Heteropoda venatoria</i>	0.1	LM	Prior	Circle	10	9	T
Young <i>et al.</i> <sup>67</sup>	2021	<i>T. senegalensis</i>	0.05–12.8	SEM	Prior	Circle	20, 50, 100	2, 5, 10	E
Greco <i>et al.</i> <sup>109</sup>	2022	<i>S. triangulosa</i> ; Artificial spider silk	1; 29 (for artificial silk)	LM	Prior	Circle	10	6	E
Yaawa <i>et al.</i> <sup>176</sup>	2022	<i>T. clavata</i>	1.7	SEM	After	Measured	5	10	E
Spizzo <i>et al.</i> <sup>48</sup>	2022	<i>C. salei</i>	1	LM	Prior	Circle	10	6	E
Arakawa <i>et al.</i> <sup>12</sup>	2022	Natural spider silks from more than 440 species	1	SEM	Prior	Circle	5	10	E
Teulè <i>et al.</i> <sup>104</sup>	2007	Artificial silk	0.001	LM	Prior	Circle	15	5	E
Brooks <i>et al.</i> <sup>177</sup>	2008	Artificial silk	0.003	LM	Prior	Circle	25–55	2	ND
Xia <i>et al.</i> <sup>105</sup>	2010	Artificial silk	ND	SEM	After	Measured	20	10	ND

TABLE I. (Continued.)

Reference	Year	Spider species	Silk collection speed (cm/s)	Diameter	Diameter measured prior or after fracture?	Cross-section evaluation	Gauge length (mm)	Strain rate (mm/min)	True or Eng. Stress-strain curve
Lin <i>et al.</i> <sup>178</sup>	2012	Artificial silk	ND	LM	Prior	Circle	20	10	ND
Xu <i>et al.</i> <sup>106</sup>	2012	Artificial silk	0.6	LM	Prior	Circle	ND	1% (gauge length) s <sup>-1</sup>	E
Albertson <i>et al.</i> <sup>179</sup>	2014	Artificial silk	0.05	LM	Prior	Circle	19	10	E
Jiang <i>et al.</i> <sup>107</sup>	2014	Artificial silk	0.02–0.13	ND	Not clearly declared	Circle	30	1	T
Heidebrecht <i>et al.</i> <sup>32</sup>	2015	Artificial silk	ND	LM	Prior	Circle	2	2.4	T
Copeland <i>et al.</i> <sup>180</sup>	2015	Artificial silk	0.001	LM	Prior	Circle	19.1	5	ND
Jones <i>et al.</i> <sup>93</sup>	2015	Artificial silk	ND	LM	Prior	Circle	19	250	ND
Lin <i>et al.</i> <sup>108</sup>	2015	Artificial silk	ND	LM	Not declared	Circle	ND	1% (gauge length) s <sup>-1</sup>	E
Perea <i>et al.</i> <sup>154</sup>	2015	Artificial silk	Artificial silk produced by a company	SEM	Prior	Circle	20	1.2	T
Weatherbee-Martin <i>et al.</i> <sup>94</sup>	2016	Artificial silk	ND	LM	Prior	Circle	10	6	E
Peng <i>et al.</i> <sup>95</sup>	2016	Artificial silk	3	LM	Prior	Circle	10	2	E
Andersson <i>et al.</i> <sup>181</sup>	2017	Artificial silk	ND	LM	Prior	Not declared	20	1	E
Madurga <i>et al.</i> <sup>182</sup>	2017	Artificial silk	5	LM	Prior	Circle	20	1	T
Thamm and Scheibel <sup>183</sup>	2017	Artificial silk	ND	LM	Prior	Circle	2	2.4	T
Madurga <i>et al.</i> <sup>184</sup>	2018	Artificial silk	5.8	LM	Prior	Circle	10	1	T
Bowen <i>et al.</i> <sup>30</sup>	2018	Artificial silk	1	LM	Prior	Circle	5	10	E
Venkatesan <i>et al.</i> <sup>78</sup>	2019	Artificial silk	ND	AFM	Prior (breaking the fiber and embedding it in resin)	Measured	20	0.5	E
Xu <i>et al.</i> <sup>185</sup>	2019	Artificial silk	ND	ND	Not declared	Circle	10	6	E
Yuan <i>et al.</i> <sup>186</sup>	2019	Artificial silk	ND	LM	Not declared	Not declared	ND	ND	ND
Wen <i>et al.</i> <sup>187</sup>	2020	Artificial silk	ND	LM	Prior	Circle	10	18	E
Zhang <i>et al.</i> <sup>188</sup>	2020	Artificial silk	ND	SEM	Prior	Circle	10	0.01	E
Tian <i>et al.</i> <sup>189</sup>	2020	Artificial silk	0.3	LM	Prior	Circle	ND	0.05% (gauge	E



TABLE I. (Continued.)

Reference	Year	Spider species	Silk collection speed (cm/s)	Diameter	Diameter measured prior or after fracture?	Cross-section evaluation	Gauge length (mm)	Strain rate (mm/min)	True or Eng. Stress-strain curve
Greco <i>et al.</i> <sup>102</sup>	2020	Artificial silk	ND	LM	Prior	Circle	10	6	E
Gonska <i>et al.</i> <sup>110</sup>	2020	Artificial silk	ND	LM	Prior	Circle	20	1	T
Zhu <i>et al.</i> <sup>190</sup>	2020	Artificial silk	5–105	LM	Prior	Circle	ND	1% (gauge length) s <sup>-1</sup>	E
Fan <i>et al.</i> <sup>96</sup>	2021	Artificial silk	ND	SEM	After	Measured	20	10	ND
Li <i>et al.</i> <sup>191</sup>	2021	Artificial silk	1	LM	Prior	Circle	10	ND	T
Saric <i>et al.</i> <sup>174</sup>	2021	Artificial silk	ND	LM	Prior	Circle	2	0.3	T
Kono <i>et al.</i> <sup>98</sup>	2021	Artificial silk	ND	SEM	Prior	Measured	5	10	E
Greco <i>et al.</i> <sup>77</sup>	2021	Artificial silk	ND	LM	Prior	Circle	10	6	E
Hu <i>et al.</i> <sup>97</sup>	2021	Artificial silk	ND	SEM	Prior	Measured	10	2	E
Asakura <i>et al.</i> <sup>192</sup>	2022	Artificial silk	ND	LM	Prior	Circle	20	3	E
Bäcklund <i>et al.</i> <sup>100</sup>	2022	Artificial silk	29–69	LM	Prior	Circle	10	6	E
Jin <i>et al.</i> <sup>193</sup>	2022	Artificial silk	ND	SEM	Prior	Measured	10	4	E
Arndt <i>et al.</i> <sup>99</sup>	2022	Artificial silk	ND	LM	Prior	Circle	10	6	E
He <i>et al.</i> <sup>194</sup>	2022	Artificial silk	4	ND	ND	ND	20	ND	ND
Asakura <i>et al.</i> <sup>195</sup>	2022	Artificial silk	ND	LM	Prior	Circle	20	3	E
Schmuck <i>et al.</i> <sup>73</sup>	2022	Artificial silk	17–69	LM	Prior	Circle	10	6	E
Cheng <i>et al.</i> <sup>196</sup>	2022	Artificial silk	ND	SEM	Prior	Circle	ND	2	E

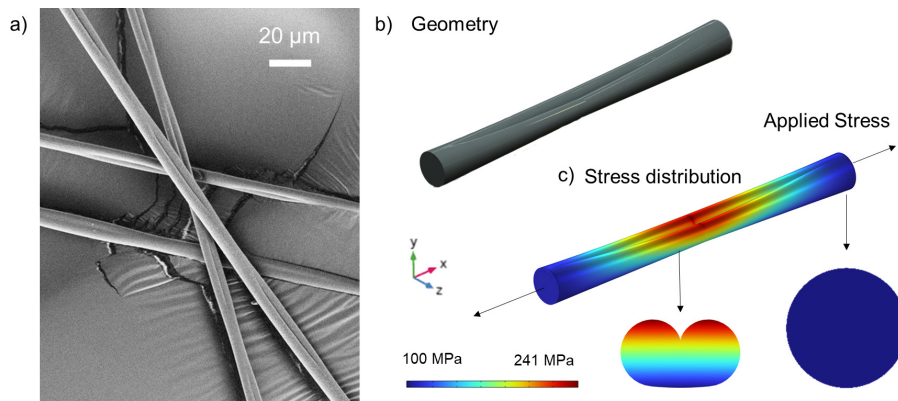


**FIG. 5.** (a) Representative SEM image of NT2RepCT fibers, which present a fairly consistent non-uniform shape, with frequent longitudinal groove regions, (b) geometrical model of these grooved regions, and (c) the consequent concentration of the stress (obtained using simulations), which is about 2.4 times the stress in the circular region/cross section, and mostly concentrated on the groove regions of high curvatures.

Unfortunately, evaluating the exact morphology of soft polymeric fibers is difficult. Light microscopy does not provide enough depth in focus to safely assess the morphological features of micrometric fibers (Fig. S6). Instead, SEM can be used to precisely evaluate the morphology of the samples,<sup>43</sup> but as mentioned above, the specific fiber sample that is used for SEM cannot be subsequently tensile tested. This means that the fiber population investigated needs to be large and homogeneous to ensure that the fibers that are tensile tested have the same shape and morphology as the one used for SEM.<sup>111</sup> When comparing data from different studies, is it therefore important to evaluate also the differences in the fibers' morphology.

The importance of having a uniform cross-section is not solely related to the calculation of the cross-sectional area, but also to the mechanical performance of the fiber. Indeed, the geometry of the structure strongly affects the local stress distribution if the fiber experiences strain.<sup>112</sup> A more homogeneous distribution of the stress is generally achieved in the absence of defects and in fibers with round cross sections.<sup>30,104</sup> To illustrate the impact of stress distribution, we have used NT2RepCT fibers. A computational study on the tensile traction of these fibers was performed (Fig. 5, supplementary material Sec. S2) in which we applied a nominal stress of about 100 MPa. The results of the simulation [Fig. 5(c)] show that there is a concentration of stress along the longitudinal groove, especially on the upper ridge. This local concentration of stress is around 2.4 times higher than the nominal stress and will result in a premature fracture of the fiber compared to a fiber with a circular cross-section of the same diameter.

The concentration of stress strongly depends on the geometry of the longitudinal groove. The local increase in stress in a section is defined by the stress concentration factor ( $K$ ) and is defined as<sup>113</sup>

$$\sigma_{max} = K\sigma_{ave},$$

where  $\sigma_{ave}$  is the average/nominal applied stress.

Through simulations, the magnitude of this concentration factor could be estimated by changing the geometry of the longitudinal groove. In this example, the sharpness of the groove is governed by its tip diameter of the tangential circumference ( $d$ ; the smaller  $d$  is, the sharper is the groove), whereas the length of the groove is  $L$  (Fig. 6). The apparent diameter of the fiber ( $D_0$ ) is measured assuming the circular cross-section by means of either light microscopy or SEM. From this, it is possible to investigate the effect of the ratio  $L/D_0$  as well as  $d/D_0$  on the stress intensity factor [Figs. 6(b) and 6(c)]. In general,  $K$

increases with the sharpness of the groove and results in a much higher local stress concentration in the fiber under traction. Moreover, the shorter the length of the groove  $L$ , the higher the concentration factor. Notably, the Poisson's ratio has little effect on the concentration of the stress when in the range between 0.1 and 0.3, which is typical for most of the solids<sup>114</sup> [Fig. 6(b), solid vs dashed lines; see also supplementary material Sec. S2 for further details].

The morphological analysis presented herein is not intended to apply to all artificial fibers, but it is used to highlight the importance of properly describing the morphology of the fibers because of its impact on fibers mechanical properties.

## METHOD FOR CALCULATING STRESS AND STRAIN

Another important factor to be considered when calculating the mechanical properties and comparing data found in the literature is how the stress and the strain were calculated. In Eqs. (1) and (2), if  $A = A_0$  and  $L = L_0$  are considered constant (initial values of the sample, i.e., nominal values)  $\sigma$  and  $\epsilon$  are commonly called engineering stress and engineering strain, respectively. Engineering stress and strain do not take into account that a fiber's cross-section is deformed during tensile testing.<sup>112</sup> In fact, during the deformation imposed by tensile strain, most materials display a secondary deformation perpendicular to the direction of loading, which is ruled by the Poisson ratio. In practice, for most materials, an applied strain on the axial direction will lead to a contraction in the transversal one. In other words, during the tensile test, the fibers are subjected to a tensile strain that will induce a reduction of their cross-sectional area.

Engineering stress and strain are defined by using the initial specimen geometry and do not consider the change in morphology, which is large in the case of silks. In contrast, true stress ( $\sigma_T$ ) and true strain ( $\epsilon_T$ ) take into account the deformation of the sample during the test, which allows the calculation of the stress and the strain with the following equations:

$$\sigma_T = \sigma(1 + \epsilon), \quad (4)$$

$$\epsilon_T = \ln(1 + \epsilon), \quad (5)$$

where  $\sigma$  and  $\epsilon$  are the engineering stress and engineering strain, respectively. This way of calculating stress and strain is commonly used in the silk field [Table I, Fig. 2(d)].

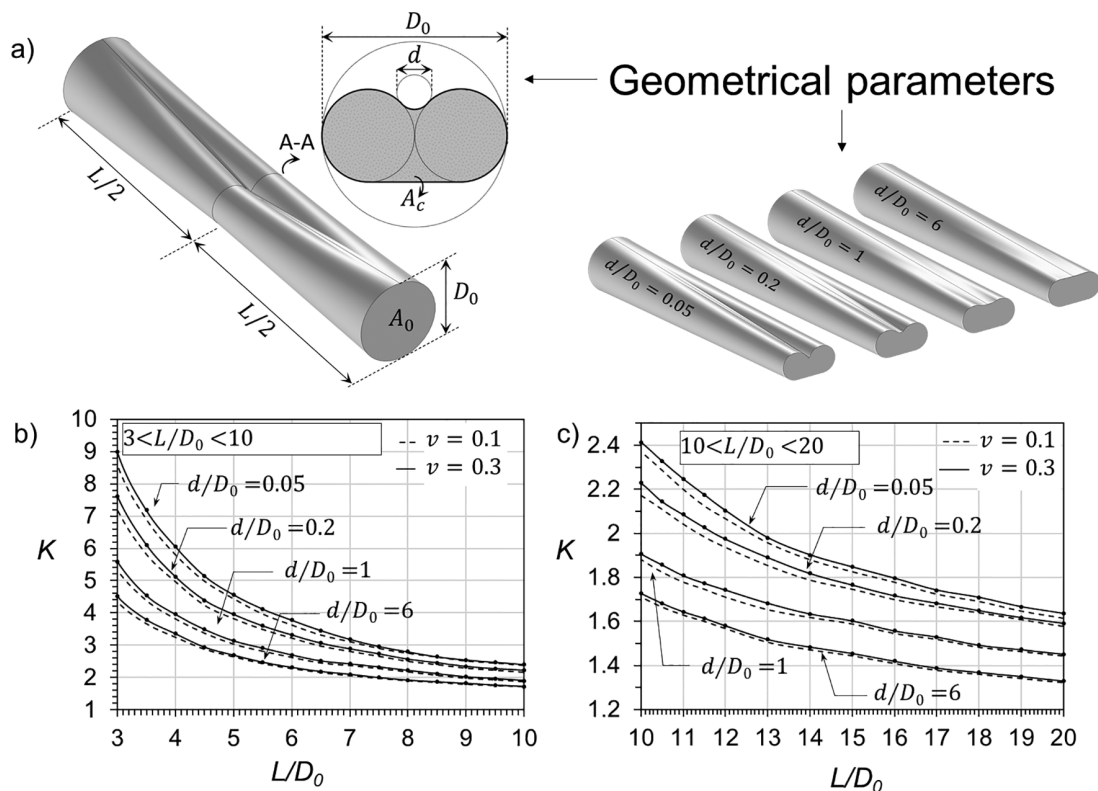


**FIG. 6.** (a) Geometrical parameters used in the simulation analysis. (b) and (c) Stress intensity factor vs the different lengths of the longitudinal groove normalized by the nominal diameter obtained with different sharpness values of such a groove. The Poisson ratios ( $\nu$ ) of the fibers have been assumed to be either 0.1 (dashed lines) or 0.3 (solid lines).

The use of such expressions for the calculation of the mechanical properties of spider silk was proposed for the first time by Guinea *et al.*<sup>115</sup> A potential problem related to this method is the assumption that the volume of the fiber is constant during the deformation, i.e., the Poisson's ratio is considered  $\nu = 0.5$  (see the supporting discussion in supplementary material Sec. S3), and that such deformation occurs homogeneously.<sup>114</sup> In Guinea *et al.*,<sup>115</sup> this assumption is supported by SEM measurements on the diameter of the stretched fibers. Nonetheless, SEM does not provide wide-length scale information, but instead only permits the analysis of precise locations that may not be representative.<sup>38</sup> Thus, the use of Eqs. (4) and (5) are not appropriate for Poisson's ratios that are different from 0.5 and when the deformation involved (i.e., strain) is large and not homogeneous. In particular, Eq. (4) should be substituted with  $\sigma_T = \sigma / (1 - \nu\epsilon)^2$  if the deformation is homogeneous (see supplementary material Sec. S3). In this context, a major problem that prevents the use of true stress and strain in silk mechanics is the necking phenomenon, which commonly occurs after the yield point and introduces strong non-uniform deformations.

Necking is commonly referred to as plastic instability and is best explained by a local growth of a thinned portion in a material on which stresses are applied.<sup>116</sup> This occurs in an unforeseeable location of the sample that is being tensile tested and is related to the presence of a local mechanical weakness that generates a concentration of stress. In solid polymers, these weaknesses can be structural defects (e.g.,

impurities) or cross-section reductions.<sup>117</sup> The necking is also visible in the stress-strain curve, where a conspicuous reduction in stress is observed after the yield point (Fig. S7). Only the data obtained from the calculation of true stress and strain before the yield point are valid and can be used directly.<sup>118</sup> After the yield point, the deformation is localized in the necking region and the stress will no longer be homogeneously distributed, causing a reduction in the load registered by the machine<sup>118</sup> [Fig. S7(b)]. Thus, when necking occurs, the deformation is non-homogeneous, and Eqs. (4) and (5) cannot be applied to calculate true stress and strain.<sup>118</sup> In order to precisely calculate the stress concentration while necking occurs, one should measure the minimal cross-section of the material during the test. Such measurements are extremely challenging and not practical for silk fibers where fracture location is unpredictable. Although engineering stress and strain do not consider the eventual reduction in cross-section due to traction, and thus are imprecise, they still represent a valid way to present data, are more easily obtained, and reduce the risk in overestimating the strength values.

Compared to the use of engineering stress and strain, the use of true stress and true strain defined in Eqs. (4) and (5) does not affect the toughness modulus and the Young's modulus, but it reduces the strain at break (Figs. 7 and S8). In addition, Eq. (4) may induce large overestimations in the stress values. To illustrate this, we generated stress-strain curves of NT2RepCT and *L. scopetarius* fibers that are

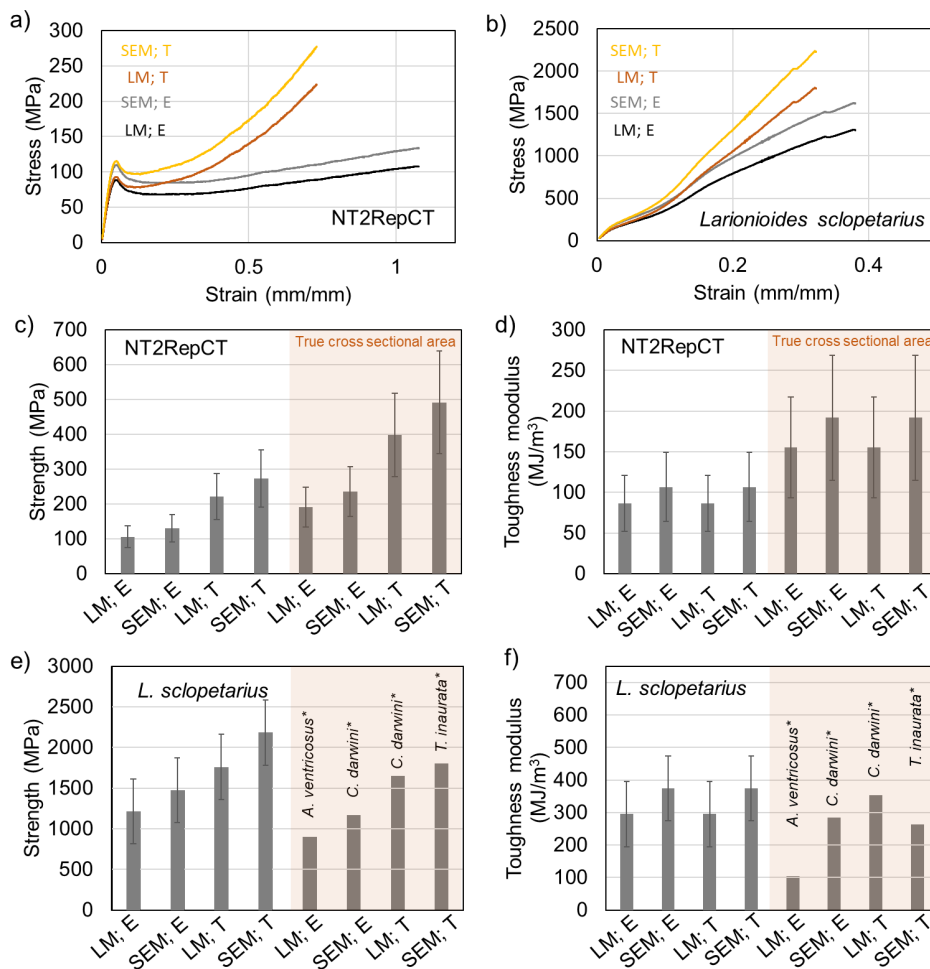


**FIG. 7.** Stress–strain curves obtained with different calculations and methods of (a) NT2RepCT fibers and (b) *L. scopetarius* spider silk. (c) Strength and (d) toughness modulus of the same set of NT2RepCT fibers calculated with different accepted methods. (e) Strength and (f) toughness modulus of the same set of *L. scopetarius* fibers calculated with different methods compared with the values taken from the literature with similar methods. LM = diameter measured with Light Microscopy; E = Engineering stress and strain; SEM = diameter measured with Scanning Electron Microscopy; T = True stress and true strain calculation. The error bars are standard deviations. \*Data obtained from Refs. 11, 52, 119, and 120.

obtained using different accepted methods (Figs. 7 and S9). This shows that if true stress/strain is calculated (we assume here  $\nu = 0.5$  for the sake of comparison), the stress is increased by almost 250% for NT2RepCT fibers and up to 80% for native silk compared to when the diameter is determined by light microscopy and engineering stress is calculated (Fig. 7). Moreover, regarding artificial spider silk with non-circular cross-sectional areas, Figs. 7(c) and 7(d) show that using the true cross-sectional area (explained in the morphology section) would increase the strength and toughness modulus by  $\sim 80\%$ .

In addition, we used the silk of *L. scopetarius* (an orb weaving spider) and determined its mechanical properties using these commonly accepted methods, as well as compared these to the mechanical properties of spider silks from the literature [Figs. 7(e) and 7(f)]. The results show that *L. scopetarius* silk is as strong and tough as the silk from *C. darwini* and *T. inaurata*, whose silk fibers are the toughest known,<sup>11,119,120</sup> when the mechanical properties are calculated using the same methods. We speculate that if the major ampullate silk from several spider species is investigated using true stress and strain, and the diameters would be determined by SEM, the properties of *C. darwini* and *T. inaurata* would not be outstanding.

Hence, caution must be used when comparing the mechanical properties of different artificial and natural silk fibers in the literature. Based on that true stress and strain entail the risk of overestimating the mechanical properties, and since the constancy in volume under different degrees of deformation is not investigated for all different silk types, engineering stress and strain seems to be the best choice when reporting the properties of silk fibers.

## CONCLUSIONS

Studies of natural and artificial spider silk fibers often rely on the fibers' mechanical properties, but as shown herein, data from different studies are frequently non-comparable due to differences in the methodological approach. We have highlighted several key parameters that greatly affect the silk fiber's mechanical properties. Based on a thorough investigation of the so-far published literature and illustrative examples, we propose that light microscopy should be used to obtain the diameter of the fibers and their cross-sectional area assumed to be circular and that the morphology should be investigated by SEM and reported. Tensile tests should be performed using a gauge length of 5–20 mm and a strain rate of 5–10 mm/min, and the data should be

processed considering engineering stress and strain. This standardized way of determining the mechanical properties of silk fibers will allow the community to produce more reproducible and comparable data. Finally, this work will also help the researchers and editors that are not experts in mechanical properties to evaluate the works where these are reported.

## MATERIALS AND METHODS

### Spinning artificial spider silk

The minispidroin NT2RepCT was obtained by recombinant protein expression with *Escherichia coli* grown in a fed-batch culture using a benchtop bioreactor as previously described.<sup>101</sup> After expression, NT2RepCT was purified under native conditions using affinity chromatography, also as described earlier.<sup>101</sup> To prepare the biomimetic spinning dope, NT2RepCT stored in a 20 mM Tris-HCl buffer at pH 8 was concentrated to 300 mg/ml with a centrifugal filter (Amicon Ultra 15) unit with 10 kDa cutoff at  $4000\times g$  and  $4^\circ\text{C}$ . Then, an optimized spinning protocol was used to manufacture artificial silk fibers from NT2RepCT.<sup>73</sup> To this end, the spinning dope was extruded at a temperature of  $22^\circ\text{C}$  and relative humidity of 30% with a flow rate of  $17\ \mu\text{l}/\text{min}$  into an 80 cm long spinning bath containing a 0.75M acetate buffer at pH 5. In the spinning bath, the liquid spinning dope formed solid fiber, which was continuously collected with a collecting speed of 58 cm/s using a rotating wheel with a circumference of 35 cm, located at the end of the spinning bath.

### Native major ampullate silk

Native major ampullate silk fibers were extracted from three adult females (mass 0.2 g) of *L. sclopetarius* at the speed of 1 cm/s. The fibers were collected into a frame and subsequently mounted on tensile tests sample holder. The fibers were by one week after they have been collected.

### Degummed *B. mori* silk

*B. mori* silk cocoons were provided by Chul Thai Silk Co., Ltd. (Phetchabun province, Thailand). For the degumming process, degumming, cocoons were cut into pieces and then boiled in two  $98^\circ\text{C}$  distilled water baths of  $\text{Na}_2\text{CO}_3$  (Sigma, USA, 1.1 and 0.4 g/l, respectively), 1.5 h each, 10 g/l. Then, they were rinsed thoroughly with warm distilled water to remove the salt and completely dried at room temperature in a laminar flow hood.

### Tensile tests

All the silk fibers were mounted on cardboard frames with a square window of  $1 \times 1\ \text{cm}^2$  (gauge length 1 cm ca). The diameters were measured by means of light microscopy and also SEM. For the latter, representative fibers were selected, and the average diameter was then used. For the former, the diameter was measured at five locations along the fiber, and the average value was then computed. In this way, each fiber possessed its mean diameter.

The samples were mounted on a 5943-Instron machine, USA, equipped with a 5N load cell. The standard used strain rate is 6 mm/min, but for the sake of the study, we also used 0.6, 60, 300, and 600 mm/min. For this work, we calculated both the true and engineering stress and strain. The Young's modulus was calculated in the initial linear elastic regime, as the slope of the fitting linear

curve. The toughness modulus was calculated as described in the paper. The fibers were tested by two weeks after they have been spun.

### Light microscopy

To investigate the fibers, two light microscopes were used. Images were collected using a Nikon Eclipse Ts2R-FL inverted microscope equipped with a DFKNME33UX264 5 MP camera and a CFI Plan Fluor DL-10X objective. Image capture was done using the Nikon NIS-Elements BR software. The other microscope was an Olympus BX61 equipped with the Olympus Steam Image Analysis software.

### Scanning electron microscopy

A Zeiss Supra-40 Field-Emission Scanning Electron Microscope was used to investigate the morphology of the fibers with the secondary electron detectors. The samples were coated with an alloy Pt: Pd (80:20) utilizing a Quora Q150 and mounted on a standard Zeiss stab.

### Statistical analysis

One-way pairwise ANOVA analysis was performed with the support of Excel<sup>®</sup>. The differences were considered significant if the two-tailed p-value was lower than 5%. The depicted error bars are standard deviations.

### Simulations

A set of numerical simulations based on finite element analysis using COMSOL Multiphysics<sup>®</sup> software was performed to find the stress concentration factor,  $K$ , as a function of geometric parameters of the imperfection. More details on the simulations can be found in supplementary material Sec. S1.

### SUPPLEMENTARY MATERIAL

In the supplementary material one can find more discussion of the methodology, as well as the analytical model regarding true stress and strain. Furthermore, in the supplementary material one can find more figures that support the findings of this paper.

### ACKNOWLEDGMENTS

We thank the reviewers for their positive comments that helped improving the manuscript. This work was supported by the Center for Innovative Medicine (CIMED) at Karolinska Institutet and Stockholm City Council, Karolinska Institutet SFO Regan (FOR 4-1364/2019) to A.R. N.M.P. and G.G. thank Professor Antonella Motta for the help with Scanning Electron Microscopy facility. N.M.P. is supported by the European Commission under the FET Proactive ("Boheme") Grant No. 863179. G.G. is supported by Wenner-Gren stiftelse (UPD2021-0047).

### AUTHOR DECLARATIONS

#### Conflict of Interest

The authors have no conflicts to disclose.



## Author Contributions

G.G. and A.R. conceived the idea. A.R. Supervised the project. B.S. produced the protein, performed spinning. G.G. conducted tensile testing and obtained fiber images with SEM and polarized light images of the fibers. S.J.K. performed the simulations and N.M.P. developed analytical models and supervised the simulation analysis. All authors contributed to the analysis and discussion of the data. G.G., B.S., and A.R. wrote the first draft of the manuscript, and all authors contributed to the editing process. All authors have given approval to the final version of the manuscript.

**Gabriele Greco:** Conceptualization (lead); Data curation (lead); Formal analysis (lead); Funding acquisition (lead); Investigation (lead); Methodology (lead); Project administration (lead); Resources (lead); Supervision (lead); Validation (lead); Visualization (lead); Writing – original draft (lead); Writing – review & editing (lead). **Benjamin Schmuck:** Data curation (supporting); Investigation (supporting); Methodology (supporting); Writing – original draft (supporting); Writing – review & editing (supporting). **Kamal Seyed Jalali:** Data curation (supporting); Investigation (supporting); Methodology (supporting); Writing – review & editing (supporting). **Nicola M. Pugno:** Methodology (supporting); Resources (supporting); Writing – review & editing (supporting). **Anna Rising:** Conceptualization (lead); Formal analysis (equal); Funding acquisition (equal); Methodology (equal); Project administration (equal); Resources (lead); Supervision (lead); Validation (equal); Visualization (equal); Writing – original draft (equal); Writing – review & editing (equal).

## DATA AVAILABILITY

The data that support the findings of this study are available within the article and its supplementary material.

## REFERENCES

- M. J. Harrington and P. Fratzl, “Natural load-bearing protein materials,” *Prog. Mater. Sci.* **120**, 100767 (2021).
- U. G. K. Wegst, H. Bai, E. Saiz, A. P. Tomsia, and R. O. Ritchie, “Bioinspired structural materials,” *Nat. Mater.* **14**(1), 23–36 (2015).
- S. J. Blamires, P. T. Spicer, and P. J. Flanagan, “Spider silk biomimetics programs to inform the development of new wearable technologies,” *Front. Mater.* **7**, 29 (2020).
- S. Salehi and T. Scheibel, “Biomimetic spider silk fibres: From vision to reality,” *Biochemist* **40**(1), 4–7 (2018).
- T. Lefèvre and M. Auger, “Spider silk as a blueprint for greener materials: A review,” *Int. Mater. Rev.* **61**(2), 127–153 (2016).
- S. Salehi, K. Koeck, and T. Scheibel, “Spider silk for tissue engineering applications,” *Molecules* **25**, 737 (2020).
- I. L. Good, J. M. Kenoyer, and R. H. Meadow, “New evidence for early silk in the Indus civilization,” *Archaeometry* **51**(3), 457–466 (2009).
- D. Kuhn, “Silk weaving in ancient China: From geometric figures to patterns of pictorial likeness,” *Chin. Sci.* **12**(12), 77–114 (1995).
- G. Greco, V. Mastellari, C. Holland, and N. M. Pugno, “Comparing modern and classical perspectives on spider silks and webs,” *Perspect. Sci.* **29**(2), 133–156 (2021).
- C. Holland, K. Numata, J. Rnjak-Kovacina, and F. P. Seib, “The biomedical use of silk: Past, present, future,” *Adv. Healthcare Mater.* **8**(1), 1800465 (2019).
- I. Agnarsson, M. Kuntner, and T. A. Blackledge, “Bioprospecting finds the toughest biological material: Extraordinary silk from a giant Riverine Orb spider,” *PLoS One* **5**(9), e11234 (2010).
- K. Arakawa, N. Kono, A. D. Malay, A. Tateishi, N. Ifuku, H. Masunaga, R. Sato, K. Tsuchiya, R. Ohtoshi, D. Pedrazzoli, T. Ichikawa, S. Fujita, M. Fujiwara, M. Tomita, and S. J. Blamires, “1000 spider silkomes: Linking sequences to silk physical properties,” *Sci. Adv.* **6**(43), eabo6043 (2022).
- C. Vepari and D. L. Kaplan, “Silk as a biomaterial,” *Prog. Polym. Sci.* **32**(8–9), 991–1007 (2007).
- L. Pan, F. Wang, Y. Cheng, W. R. Leow, Y. W. Zhang, M. Wang, P. Cai, B. Ji, D. Li, and X. Chen, “A supertough electro-tendon based on spider silk composites,” *Nat. Commun.* **11**(1), 1332 (2020).
- B. Xu, Y. Yang, Y. Yan, and B. Zhang, “Bionics design and dynamics analysis of space webs based on spider predation,” *Acta Astronaut.* **159**, 294–307 (2019).
- T. Yoshioka, T. Tsubota, K. Tashiro, A. Jouraku, and T. Kameda, “A study of the extraordinarily strong and tough silk produced by bagworms,” *Nat. Commun.* **10**(1), 1469 (2019).
- Y. Yang, G. Greco, D. Maniglio, B. Mazzolai, C. Migliaresi, N. Pugno, and A. Motta, “Spider (*Linothele megalheloides*) and silkworm (*Bombyx mori*) silks: Comparative physical and biological evaluation,” *Mater. Sci. Eng. C* **107**, 110197 (2020).
- A. Dellaquila, G. Greco, E. Campodoni, M. Mazzocchi, B. Mazzolai, A. Tampieri, N. M. Pugno, and M. Sandri, “Optimized production of a high-performance hybrid biomaterial: Biomaterialized spider silk for bone tissue engineering,” *J. Appl. Polym. Sci.* **137**(22), 48739 (2020).
- K. Z. Htut, A. M. Alicea-serrano, S. Singla, I. Agnarsson, J. E. Garb, M. Kuntner, R. A. Haney, M. Marhabaie, T. A. Blackledge, A. Dhinojwala, and A. Dhinojwala, “Correlation between protein secondary structure and mechanical performance for the ultra-tough dragline silk of Darwin’s bark spider,” *J. R. Soc. Interface* **18**, 20210320 (2021).
- G. Greco and N. M. Pugno, “How spiders hunt heavy prey: The tangle web as a pulley and spider’s lifting mechanics observed and quantified in the laboratory,” *J. R. Soc. Interface* **18**(175), 20200907 (2021).
- L. Kundanati, N. G. D. Novo, G. Greco, G. Greco, S. Siboni, and C. D. Volpe, “Multifunctional roles of hairs and spines in old man of the Andes cactus: Droplet distant coalescence and mechanical strength,” *Phys. Fluids* **34**, 012003 (2022).
- R. Guarino, G. Greco, B. Mazzolai, and N. M. Pugno, “Fluid-structure interaction study of spider’s hair flow-sensing system,” *Mater. Today Proc.* **7**, 418–425 (2019).
- M. Benzarti, M. Ben Tkaya, C. Pailler Mattei, and H. Zahouani, “Hair mechanical properties depending on age and origin,” *World Acad. Sci. Eng. Technol.* **50**, 466–472 (2011).
- D. S. Fudge and J. M. Gosline, “Molecular design of the  $\alpha$ -keratin composite: Insights from a matrix-free model, hagfish slime threads,” *Proc. R. Soc. B* **271**(1536), 291–299 (2004).
- A. H. Barber, D. Lu, and N. M. Pugno, “Extreme strength observed in limpet teeth,” *J. R. Soc. Interface* **12**(105), 20141326 (2015).
- E. Carrington and J. M. Gosline, “Mechanical design of mussel byssus: Load cycle and strain rate dependence,” *Amal. Malacol. Bull.* **18**, 135–142 (2004).
- J. M. Gosline, P. A. Guerette, C. S. Ortlepp, and K. N. Savage, “The mechanical design of spider silks: From fibroin sequence to mechanical function,” *J. Exp. Biol.* **202**, 3295–3303 (1999).
- C. M. Pollock and R. E. Shadwick, “Relationship between body mass and biomechanical properties of limb tendons in adult mammals,” *Am. J. Physiol. - Regul., Integr. Comp. Physiol.* **266**(3), R1016–R1021 (1994).
- M. Feughelman, “Mechanical hysteresis in wool keratin fibers,” *J. Macromol. Sci. Part B* **38**, 37–41 (1999).
- C. H. Bowen, B. Dai, C. J. Sargent, W. Bai, P. Ladiwala, H. Feng, W. Huang, D. L. Kaplan, J. M. Galazka, and F. Zhang, “Recombinant spidroins fully replicate primary mechanical properties of natural spider silk,” *Biomacromolecules* **19**, 3853–3860 (2018).
- L. Xu, T. Lefèvre, K. E. Orrell, Q. Meng, M. Auger, X. Q. Liu, and J. K. Rainey, “Structural and mechanical roles for the C-terminal nonrepetitive domain become apparent in recombinant spider aciniform silks,” *Biomacromolecules* **18**(11), 3678–3686 (2017).
- A. Heidebrecht, L. Eisoldt, J. Diehl, A. Schmidt, M. Geffers, G. Lang, and T. Scheibel, “Biomimetic fibers made of recombinant spidroins with the same toughness as natural spider silk,” *Adv. Mater.* **27**(13), 2189–2194 (2015).

- <sup>33</sup>J. E. Gordon, *The Science of Structures and Materials* (Times Books, New York, 1988).
- <sup>34</sup>F. Xu, C. Yan, Y. T. Shyng, H. Chang, Y. Xia, and Y. Zhu, "Ultra-toughened nylon 12 nanocomposites reinforced with IF-WS2," *Nanotechnology* **25**(32), 325701 (2014).
- <sup>35</sup>R. Kumar, L. P. Mikkelsen, H. Lilholt, and B. Madsen, "Understanding the mechanical response of glass and carbon fibres: Stress-strain analysis and modulus determination," *IOP Conf. Ser. Mater. Sci. Eng.* **942**(1), 012033 (2020).
- <sup>36</sup>D. Lawlor, *Introduction to Light Microscopy*, 1st ed. (Springer, Cham, 2019).
- <sup>37</sup>M. Born and E. Wolf, *Principles of Optics* (Cambridge University Press, 1999).
- <sup>38</sup>T. A. Blackledge, R. A. Cardullo, and C. Y. Hayashi, "Polarized light microscopy, variability in spider silk diameters, and the mechanical characterization of spider silk," *Invertebr. Biol.* **124**(2), 165–173 (2005).
- <sup>39</sup>F. Perez-Miles, *New World Tarantulas*, 1st ed. (Springer Nature, Switzerland, 2020).
- <sup>40</sup>F. Perez-Miles and D. Ortiz-Villatoro, "Tarantulas do not shoot silk from their legs: Experimental evidence in four species of new world tarantulas," *J. Exp. Biol.* **215**(10), 1749–1752 (2012).
- <sup>41</sup>D. Stengel, J. B. Addison, D. Onofrei, N. U. Huynh, G. Youssef, and G. P. Holland, "Hydration-induced  $\beta$ -sheet crosslinking of  $\alpha$ -helical-rich spider prey-wrapping silk," *Adv. Funct. Mater.* **31**(13), 2007161 (2021).
- <sup>42</sup>M. Wirth, J. O. Wolff, E. Appel, and S. N. Gorb, "Ultrastructure of spider thread anchorages," *J. Morphol.* **280**(4), 534–543 (2019).
- <sup>43</sup>J. I. Goldstein, D. E. Newbury, J. R. Michael, N. W. M. Ritchie, J. H. J. Scott, and D. C. Joy, *Scanning Electron Microscopy and X-Ray Microanalysis*, 4th ed. (Springer, New York, 2018).
- <sup>44</sup>H. Schatten and J. Pawley, *Biological Low-Voltage Scanning Electron Microscopy* (Springer, 2008).
- <sup>45</sup>Y. Zhang, T. Huang, D. M. Jorgens, A. Nickerson, L. J. Lin, J. Pelz, J. W. Gray, C. S. López, and X. Nan, "Quantitating morphological changes in biological samples during scanning electron microscopy sample preparation with correlative super-resolution microscopy," *PLoS One* **12**(5), e0176839 (2017).
- <sup>46</sup>J. Kuo, *Electron Microscopy* (Humana Press Inc., New Jersey, 2007).
- <sup>47</sup>J. R. Williams and A. A. Clifford, *Supercritical Fluid—Methods and Protocols* (Humana Press Inc., New Jersey, 2000).
- <sup>48</sup>F. Spizzo, G. Greco, L. Bianco, M. Coisson, and N. M. Pugno, "Magnetostrictive and electroconductive stress-sensitive functional spider silk," *Adv. Funct. Mater.* **32**, 2207382 (2022).
- <sup>49</sup>R. W. WORK, "Viscoelastic behaviour and wet supercontraction of major ampullate silk fibres of certain orb-web-building spiders (*Araneae*)," *J. Exp. Biol.* **118**(1), 379–404 (1985).
- <sup>50</sup>T. A. Blackledge, J. E. Swindeman, and C. Y. Hayashi, "Quasistatic and continuous dynamic characterization of the mechanical properties of silk from the cobweb of the black widow spider *Latrodectus hesperus*," *J. Exp. Biol.* **208**(10), 1937–1949 (2005).
- <sup>51</sup>I. Krasnov, I. Diddens, N. Hauptmann, G. Helms, M. Ogurreck, T. Seydel, S. S. Funari, and M. Müller, "Mechanical properties of silk: Interplay of deformation on macroscopic and molecular length scales," *Phys. Rev. Lett.* **100**(4), 048104 (2008).
- <sup>52</sup>L. Cheng, J. Shao, F. Wang, Z. Li, and F. Dai, "Strain rate dependent mechanical behavior of *B. Mori* silk, *A. assama* silk, *A. Pernyi* silk and *A. Ventricosus* spider silk," *Mater. Des.* **195**, 108988 (2020).
- <sup>53</sup>L. Eisoldt, A. Smith, and T. Scheibel, "Decoding the secrets of spider silk," *Mater. Today* **14**(3), 80–86 (2011).
- <sup>54</sup>F. Vollrath, "Biology of spider silk," *Int. J. Biol. Macromol.* **24**(2–3), 81–88 (1999).
- <sup>55</sup>M. A. Meyers and K. K. Chawla, *Mechanical Behaviour of Materials* (Cambridge University Press, Cambridge, 2009).
- <sup>56</sup>R. Lakes, *Viscoelastic Materials* (Cambridge University Press, New York, 2009).
- <sup>57</sup>M. W. Denny, "The physical properties of spider's silk and their role in the design of orb-webs," *J. Exp. Biol.* **65**, 483–506 (1976).
- <sup>58</sup>K. Yazawa, A. D. Malay, H. Masunaga, Y. Norma-Rashid, and K. Numata, "Simultaneous effect of strain rate and humidity on the structure and mechanical behavior of spider silk," *Commun. Mater.* **1**(1), 10 (2020).
- <sup>59</sup>I. Ahmad, A. Baharum, and I. Abdullah, "Effect of extrusion rate and fiber loading on mechanical properties of Twaron fiber-thermoplastic natural rubber (TPNR) composites," *J. Reinf. Plast. Compos.* **25**(9), 957–965 (2006).
- <sup>60</sup>W. Yang, Y. Yu, O. Robert, M. A. Meyers, W. Yang, Y. Yu, R. O. Ritchie, and M. A. Meyers, "On the strength of hair across species on the strength of hair across species," *Matter* **2**(1), 136–149 (2019).
- <sup>61</sup>H. C. Kim, D. Kim, J. Y. Lee, L. Zhai, and J. Kim, "Effect of wet spinning and stretching to enhance mechanical properties of cellulose nanofiber filament," *Int. J. Precis. Eng. Manuf. - Green Technol.* **6**(3), 567–575 (2019).
- <sup>62</sup>G. M. Swallowe, *Mechanical Properties and Testing of Polymers* (Springer, 1999).
- <sup>63</sup>T. W. Huseby and S. Matsuoka, "Mechanical properties solid liquid polymers," *Mater. Sci. Eng.* **1**, 321 (1967).
- <sup>64</sup>D. C. Kong, M. H. Yang, X. S. Zhang, Z. C. Du, Q. Fu, X. Q. Gao, and J. W. Gong, "Control of polymer properties by entanglement: A review," *Macromol. Mater. Eng.* **306**(12), 2100536 (2021).
- <sup>65</sup>J. Yao, S. Chen, Y. Chen, B. Wang, Q. Pei, and H. Wang, "Macrofibers with high mechanical performance based on aligned bacterial cellulose nanofibers," *ACS Appl. Mater. Interfaces* **9**(24), 20330–20339 (2017).
- <sup>66</sup>F. Vollrath, B. Madsen, and Z. Shao, "The effect of spinning conditions on the mechanics of a spider's dragline silk," *Proc. R. Soc. B* **268**(1483), 2339–2346 (2001).
- <sup>67</sup>R. J. Young, C. Holland, Z. Shao, and F. Vollrath, "Spinning conditions affect structure and properties of Nephila spider silk," *MRS Bull.* **46**(10), 915–924 (2021).
- <sup>68</sup>P. M. Cunniff, S. A. Fossey, M. A. Auerbach, J. W. Song, D. L. Kaplan, W. W. Adams, R. K. Eby, D. Mahoney, and D. L. Vezie, "Mechanical and thermal properties of dragline silk from the spider *Nephila clavipes*," *Polym. Adv. Technol.* **5**(8), 401–410 (1994).
- <sup>69</sup>K. Yazawa and U. Sasaki, "Forcibly spun dragline silk fibers from web-building spider *Trichonephila clavata* ensure robustness irrespective of spinning speed and humidity," *Int. J. Biol. Macromol.* **168**, 550–557 (2021).
- <sup>70</sup>K. Yazawa, Y. Tatebayashi, and Z. Kajiura, "Eri silkworm spins mechanically robust silk fibers regardless of reeling speed," *J. Exp. Biol.* **225**(3), jeb243458 (2022).
- <sup>71</sup>M. Elices, G. V. Guinea, G. R. Plaza, J. I. Real, and J. Pérez-Rigueiro, "Example of microprocessing in a natural polymeric fiber: Role of reeling stress in spider silk," *J. Mater. Res.* **21**(8), 1931–1938 (2006).
- <sup>72</sup>J. Pérez-Rigueiro, "The effect of spinning forces on spider silk properties," *J. Exp. Biol.* **208**(14), 2633–2639 (2005).
- <sup>73</sup>B. Schmuck, G. Greco, F. G. Bäcklund, N. M. Pugno, J. Johansson, and A. Rising, "Impact of physio-chemical spinning conditions on the mechanical properties of biomimetic spider silk fibers," *Commun. Mater.* **3**, 83 (2022).
- <sup>74</sup>A. D. Parkhe, S. K. Seeley, K. Gardner, L. Thompson, and R. V. Lewis, "Structural studies of spider silk proteins in the fiber," *J. Mol. Recognit.* **10**(1), 1–6 (1997).
- <sup>75</sup>Y. Liu, Z. Shao, and F. Vollrath, "Relationships between supercontraction and mechanical properties of spider silk," *Nat. Mater.* **4**(12), 901–905 (2005).
- <sup>76</sup>M. Elices, G. R. Plaza, J. Pérez-Rigueiro, and G. V. Guinea, "The hidden link between supercontraction and mechanical behavior of spider silks," *J. Mech. Behav. Biomed. Mater.* **4**(5), 658–669 (2011).
- <sup>77</sup>G. Greco, T. Arndt, B. Schmuck, J. Francis, F. G. Bäcklund, O. Shilkova, A. Barth, N. Gonska, G. Seisenbaeva, V. Kessler, J. Johansson, N. M. Pugno, and A. Rising, "Tyrosine residues mediate supercontraction in biomimetic spider silk," *Commun. Mater.* **2**, 43 (2021).
- <sup>78</sup>H. Venkatesan, J. Chen, H. Liu, Y. Kim, S. Na, W. Liu, and J. Hu, "Artificial spider silk is smart like natural one: Having humidity-sensitive shape memory with superior recovery stress," *Mater. Chem. Front.* **3**(11), 2472–2482 (2019).
- <sup>79</sup>C. Boutry and T. A. Blackledge, "Evolution of supercontraction in spider silk: Structure-function relationship from tarantulas to orb-weavers," *J. Exp. Biol.* **213**(20), 3505–3514 (2010).
- <sup>80</sup>T. Giesa, R. Schuetz, P. Fratzl, M. J. Buehler, and A. Masic, "Unraveling the molecular requirements for macroscopic silk supercontraction," *ACS Nano* **11**(10), 9750–9758 (2017).
- <sup>81</sup>J. R. White, "Polymer ageing: Physics, chemistry or engineering? time to reflect," *C. R. Chim.* **9**(11–12), 1396–1408 (2006).
- <sup>82</sup>R. Minguez, L. Barrenetxea, E. Solaberrieta, and E. Lizundia, "A simple approach to understand the physical aging in polymers," *Eur. J. Phys.* **40**(1), 015502 (2019).

- <sup>83</sup>L. C. Brinson and T. S. Gates, "Effects of physical aging on long term creep of polymers and polymer matrix composites," *Int. J. Solids Struct.* **32**(6–7), 827–846 (1995).
- <sup>84</sup>B. R. Frieberg, E. Glynos, G. Sakellariou, M. Tyagi, and P. F. Green, "Effect of molecular stiffness on the physical aging of polymers," *Macromolecules* **53**(18), 7684–7690 (2020).
- <sup>85</sup>E. Lepore, M. Isaia, S. Mammola, and N. Pugno, "The effect of ageing on the mechanical properties of the silk of the bridge spider *Larinioides cornutus* (Clerck, 1757)," *Sci. Rep.* **6**, 24699 (2016).
- <sup>86</sup>Z. Shao and F. Vollrath, "Surprising strength of silkworm silk," *Nature* **418**(6899), 741 (2002).
- <sup>87</sup>N. Kono, H. Nakamura, A. Tateishi, K. Numata, and K. Arakawa, "The balance of crystalline and amorphous regions in the fibroin structure underpins the tensile strength of bagworm silk," *Zool. Lett.* **7**(1), 11 (2021).
- <sup>88</sup>N. Kong, F. Wan, W. Dai, P. Wu, C. Su, C. Peng, K. Zheng, X. Chen, S. Ling, J. Gong, and Y. Yao, "A cuboid spider silk: Structure–function relationship and polypeptide signature," *Macromol. Rapid Commun.* **41**(6), 1900583 (2020).
- <sup>89</sup>I. C. Um, H. Y. Kweon, K. G. Lee, D. W. Ihm, J. H. Lee, and Y. H. Park, "Wet spinning of silk polymer. I. Effect of coagulation conditions on the morphological feature of filament," *Int. J. Biol. Macromol.* **34**(1–2), 89–105 (2004).
- <sup>90</sup>C. Huang, H. Niu, J. Wu, Q. Ke, X. Mo, and T. Lin, "Needleless electrospinning of polystyrene fibers with an oriented surface line texture," *J. Nanomater.* **2012**, 473872.
- <sup>91</sup>W. Liu, C. Huang, and X. Jin, "Electrospinning of grooved polystyrene fibers: Effect of solvent systems," *Nanoscale Res. Lett.* **10**(1), 237 (2015).
- <sup>92</sup>T. Nakajima, *Advanced Fiber Spinning Technology* (Woodhead Publishing Limited, Cambridge, 1994).
- <sup>93</sup>J. A. Jones, T. I. Harris, C. L. Tucker, K. R. Berg, S. Y. Christy, B. A. Day, D. A. Gaztambide, N. J. C. Needham, A. L. Ruben, P. F. Oliveira, R. E. Decker, and R. V. Lewis, "More than just fibers: An aqueous method for the production of innovative recombinant spider silk protein materials," *Biomacromolecules* **16**(4), 1418–1425 (2015).
- <sup>94</sup>N. Weatherbee-Martin, L. Xu, A. Hupe, L. Kreplak, D. S. Fudge, X. Q. Liu, and J. K. Rainey, "Identification of wet-spinning and post-spin stretching methods amenable to recombinant spider aciniform silk," *Biomacromolecules* **17**(8), 2737–2746 (2016).
- <sup>95</sup>Q. Peng, Y. Zhang, L. Lu, H. Shao, K. Qin, X. Hu, and X. Xia, "Recombinant spider silk from aqueous solutions via a bio-inspired microfluidic chip," *Sci. Rep.* **6**, 36473 (2016).
- <sup>96</sup>T. Fan, R. Qin, Y. Zhang, J. Wang, J. S. Fan, X. Bai, W. Yuan, W. Huang, S. Shi, X. C. Su, D. Yang, and Z. Lin, "Critical role of minor eggcase silk component in promoting spidroin chain alignment and strong fiber formation," *Proc. Natl. Acad. Sci. U. S. A.* **118**(38), e2100496118 (2021).
- <sup>97</sup>C. F. Hu, Z. G. Qian, Q. Peng, Y. Zhang, and X. X. Xia, "Unconventional spidroin assemblies in aqueous dope for spinning into tough synthetic fibers," *ACS Biomater. Sci. Eng.* **7**(8), 3608–3617 (2021).
- <sup>98</sup>N. Kono, H. Nakamura, M. Mori, Y. Yoshida, R. Ohtoshi, A. D. Malay, D. A. Pedrazzoli Moran, M. Tomita, K. Numata, and K. Arakawa, "Multicomponent nature underlies the extraordinary mechanical properties of spider dragline silk," *Proc. Natl. Acad. Sci. U. S. A.* **118**(31), e2107065118 (2021).
- <sup>99</sup>T. Arndt, G. Greco, B. Schmuck, J. Bunz, O. Shilkova, J. Francis, N. M. Pugno, K. Jaudzems, A. Barth, J. Johansson, and A. Rising, "Engineered spider silk proteins for biomimetic spinning of fibers with toughness equal to dragline silks," *Adv. Funct. Mater.* **32**, 2200986 (2022).
- <sup>100</sup>F. G. Bäcklund, B. Schmuck, G. H. B. Miranda, G. Greco, N. M. Pugno, J. Ryd, and A. Rising, "An image-analysis-based method for the prediction of recombinant protein fiber tensile strength," *Materials* **15**(708), 708 (2022).
- <sup>101</sup>B. Schmuck, G. Greco, A. Barth, N. M. Pugno, J. Johansson, and A. Rising, "High-yield production of a super-soluble miniature spidroin for biomimetic high-performance materials," *Mater. Today* **50**, 16 (2021).
- <sup>102</sup>G. Greco, J. Francis, T. Arndt, B. Schmuck, F. G. Bäcklund, A. Barth, J. Johansson, N. M. Pugno, and A. Rising, "Properties of biomimetic artificial spider silk fibers tuned by postspin bath incubation," *Molecules* **25**, 3248 (2020).
- <sup>103</sup>Z. You, X. Ye, L. Ye, Q. Qian, M. Wu, J. Song, J. Che, and B. Zhong, "Extraordinary mechanical properties of composite silk through hereditary transgenic silkworm expressing recombinant major ampullate spidroin," *Sci. Rep.* **8**(1), 15956 (2018).
- <sup>104</sup>F. Teulé, W. A. Furin, A. R. Cooper, J. R. Duncan, and R. V. Lewis, "Modifications of spider silk sequences in an attempt to control the mechanical properties of the synthetic fibers," *J. Mater. Sci.* **42**(21), 8974–8985 (2007).
- <sup>105</sup>X.-X. Xia, Z.-G. Qian, C. S. Ki, Y. H. Park, D. L. Kaplan, and S. Y. Lee, "Native-sized recombinant spider silk protein produced in metabolically engineered *Escherichia coli* results in a strong fiber," *Proc. Natl. Acad. Sci.* **107**(32), 14059–14063 (2010).
- <sup>106</sup>L. Xu, J. K. Rainey, Q. Meng, and X. Q. Liu, "Recombinant minimalist spider wrapping silk proteins capable of native-like fiber formation," *PLoS One* **7**(11), e50227 (2012).
- <sup>107</sup>P. Jiang, N. Mari-Buyé, R. Madurga, M. Arroyo-Hernández, C. Solanas, A. Gañán, R. Daza, G. R. Plaza, G. V. Guinea, M. Elices, J. L. Cenis, and J. Pérez-Rigueiro, "Spider silk gut: Development and characterization of a novel strong spider silk fiber," *Sci. Rep.* **4**, 7326 (2014).
- <sup>108</sup>S. Lin, S. Ryu, O. Tokareva, G. Gronau, M. M. Jacobsen, W. Huang, D. J. Rizzo, D. Li, C. Staii, N. M. Pugno, J. Y. Wong, D. L. Kaplan, and M. J. Buehler, "Predictive modelling-based design and experiments for synthesis and spinning of bioinspired silk fibres," *Nat. Commun.* **6**, 6592 (2015).
- <sup>109</sup>G. Greco, H. Mirbaha, B. Schmuck, A. Rising, and N. M. Pugno, "Artificial and natural silk materials have high mechanical property variability regardless of sample size," *Sci. Rep.* **12**(1), 3507 (2022).
- <sup>110</sup>N. Gonska, P. A. López, P. Lozano-Picazo, M. Thorpe, G. V. Guinea, J. Johansson, A. Barth, J. Pérez-Rigueiro, and A. Rising, "Structure–function relationship of artificial spider silk fibers produced by straining flow spinning," *Biomacromolecules* **21**(6), 2116–2124 (2020).
- <sup>111</sup>P. Echlin, *Handbook of Sample Preparation for Scanning Electron Microscopy and X-ray Microanalysis* (Springer, New York, 2009).
- <sup>112</sup>B. J. Goodno and J. M. Gere, *Mechanics of Materials*, 9th ed. (Cengage Learning Emea, 2020).
- <sup>113</sup>W. D. Pilkey, D. F. Pilkey, and Z. Bi, *Peterson's Stress Concentration Factors* (John Wiley & Sons Inc., 2020).
- <sup>114</sup>B. J. Goodno and J. M. Gere, *Mechanics of Materials* (Cengage Learning, Boston, 2018).
- <sup>115</sup>G. V. Guinea, J. Pérez-Rigueiro, G. R. Plaza, and M. Elices, "Volume constancy during stretching of spider silk," *Biomacromolecules* **7**(7), 2173–2177 (2006).
- <sup>116</sup>R. Séguela, "On the natural draw ratio of semi-crystalline polymers: Review of the mechanical, physical and molecular aspects," *Macromol. Mater. Eng.* **292**, 235–244 (2007).
- <sup>117</sup>I. M. Ward, *Mechanical Properties of Solid Polymers* (Wiley Interscience, New York, 1980).
- <sup>118</sup>S. Tu, X. Ren, J. He, and Z. Zhang, "Stress strain curves of metallic materials and post-necking strain hardening," *Fatigue Fract. Eng. Mater. Struct.* **43**, 3–19 (2019).
- <sup>119</sup>G. V. Guinea, M. Elices, G. R. Plaza, G. B. Perea, R. Daza, C. Riekel, F. Agulló-Rueda, C. Hayashi, Y. Zhao, and J. Pérez-Rigueiro, "Minor ampullate silks from Nephila and Argiope spiders: Tensile properties and microstructural characterization," *Biomacromolecules* **13**(7), 2087–2098 (2012).
- <sup>120</sup>N. Kono, R. Ohtoshi, A. D. Malay, M. Mori, H. Masunaga, Y. Yoshida, H. Nakamura, K. Numata, and K. Arakawa, "Darwin's bark spider shares a spidroin repertoire with *Caerostris extrusa* but achieves extraordinary silk toughness through gene expression," *Open Biol.* **11**(12), 210242 (2021).
- <sup>121</sup>R. S. I. Wilson, "The control of dragline spinning in the garden spider," *Quart. J. Microsc. Sci. Ser.* **3**(104), 557–571 (1962).
- <sup>122</sup>W. Work, "The force-elongation behavior of web fibers and silks forcibly obtained from orb web spinning spiders," *Text. Res. J.* **46**(7), 485–492 (1976).
- <sup>123</sup>R. W. Work, "Dimensions, birefringences, and force-elongation behavior of major and minor ampullate silk fibers from orb-web-spinning spiders—The effects of wetting on these properties," *Text. Res. J.* **47**(10), 650–662 (1977).
- <sup>124</sup>J. M. Gosline, M. E. DeMont, and M. W. Denny, "The structure and properties of spider silk," *Endeavour* **10**(1), 37–43 (1986).
- <sup>125</sup>Z. Shao and F. Vollrath, "The effect of solvents on spider silk studied by mechanical testing and single-fibre Raman spectroscopy," *Int. J. Biol. Macromol.* **24**, 295–300 (1999).



- <sup>126</sup>Z. Shao and F. Vollrath, "The effect of solvents on the contraction and mechanical properties of spider silk," *Polymers* **40**(7), 1799–1806 (1999).
- <sup>127</sup>B. Madsen, Z. Z. Shao, and F. Vollrath, "Variability in the mechanical properties of spider silks on three levels: Interspecific, intraspecific and intra-individual," *Int. J. Biol. Macromol.* **24**(2–3), 301–306 (1999).
- <sup>128</sup>J. Pérez-Rigueiro, M. Elices, J. Llorca, and C. Viney, "Tensile properties of *Argiope trifasciata* drag line silk obtained from the spider's web," *J. Appl. Polym. Sci.* **82**(9), 2245–2251 (2001).
- <sup>129</sup>A. Lazaris, S. Arcidiacono, Y. Huang, J. F. Zhou, F. Duguay, N. Chretien, E. A. Welsh, J. W. Soares, and C. N. Karatzas, "Spider silk fibers spun from soluble recombinant silk produced in mammalian cells," *Science* **295**(5554), 472–476 (2002).
- <sup>130</sup>G. V. Guinea, M. Elices, J. Pérez-Rigueiro, and G. Plaza, "Self-tightening of spider silk fibers induced by moisture," *Polymers* **44**(19), 5785–5788 (2003).
- <sup>131</sup>F. K. Ko and J. Jovicic, "Modeling of mechanical properties and structural design of spider web," *Biomacromolecules* **5**(3), 780–785 (2004).
- <sup>132</sup>G. V. Guinea, "Stretching of supercontracted fibers: A link between spinning and the variability of spider silk," *J. Exp. Biol.* **208**(1), 25–30 (2005).
- <sup>133</sup>Y. Yang, X. Chen, Z. Shao, P. Zhou, D. Porter, D. P. Knight, and F. Vollrath, "Toughness of spider silk at high and low temperatures," *Adv. Mater.* **17**(1), 84–88 (2005).
- <sup>134</sup>T. A. Blackledge and C. Y. Hayashi, "Silken toolkits: Biomechanics of silk fibers spun by the orb web spider *Argiope argentata* (Fabricius 1775)," *J. Exp. Biol.* **209**, 2452–2461 (2006).
- <sup>135</sup>B. O. Swanson, T. A. Blackledge, J. Beltrán, and C. Y. Hayashi, "Variation in the material properties of spider dragline silk across species," *Appl. Phys. A: Mater. Sci. Process.* **82**(2), 213–218 (2006).
- <sup>136</sup>J. Pérez-Rigueiro, M. Elices, G. R. Plaza, J. Rueda, and G. V. Guinea, "Fracture surfaces and tensile properties of UV-irradiated spider silk fibers," *J. Polym. Sci., Part B: Polym. Phys.* **45**, 786–793 (2007).
- <sup>137</sup>I. Agnarsson, C. Boutry, and T. A. Blackledge, "Spider silk aging: Initial improvement in a high performance material followed by slow degradation," *J. Exp. Zool., Part A: Ecol. Genet. Physiol.* **309**(8), 494–504 (2008).
- <sup>138</sup>K. N. Savage and J. M. Gosline, "The effect of proline on the network structure of major ampullate silks as inferred from their mechanical and optical properties," *J. Exp. Biol.* **211**(12), 1937–1947 (2008).
- <sup>139</sup>C. Ortlepp and J. M. Gosline, "The scaling of safety factor in spider draglines," *J. Exp. Biol.* **211**(17), 2832–2840 (2008).
- <sup>140</sup>S. M. Lee, E. Pippel, U. Gösele, C. Dresbach, Y. Qin, C. V. Chandran, T. Bräuniger, G. Hause, and M. Knez, "Greatly increased toughness of infiltrated spider silk," *Science* **324**(5926), 488–492 (2009).
- <sup>141</sup>A. Sensenig, I. Agnarsson, and T. A. Blackledge, "Behavioural and biomaterial coevolution in spider orb webs," *J. Evol. Biol.* **23**(9), 1839–1856 (2010).
- <sup>142</sup>G. V. Guinea, M. Cerdeira, G. R. Plaza, M. Elices, and J. Pérez-Rigueiro, "Recovery in viscid line fibers," *Biomacromolecules* **11**(5), 1174–1179 (2010).
- <sup>143</sup>A. T. Sensenig, I. Agnarsson, and T. A. Blackledge, "Adult spiders use tougher silk: Ontogenetic changes in web architecture and silk biomechanics in the orb-weaver spider," *J. Zool.* **285**(1), 28–38 (2011).
- <sup>144</sup>E. M. Pogozelski, W. L. Becker, B. D. See, and C. M. Kieffer, "Mechanical testing of spider silk at cryogenic temperatures," *Int. J. Biol. Macromol.* **48**(1), 27–31 (2011).
- <sup>145</sup>M. Hudspeth, X. Nie, W. Chen, and R. Lewis, "Effect of loading rate on mechanical properties and fracture morphology of spider silk," *Biomacromolecules* **13**(8), 2240–2246 (2012).
- <sup>146</sup>S. J. Blamires, C.-L. Wu, T. A. Blackledge, and I.-M. Tso, "Post-secretion processing influences spider silk performance," *J. R. Soc. Interface* **9**(75), 2479–2487 (2012).
- <sup>147</sup>T. A. Blackledge, J. Pérez-Rigueiro, G. R. Plaza, B. Perea, A. Navarro, G. V. Guinea, and M. Elices, "Sequential origin in the high performance properties of orb spider dragline silk," *Sci. Rep.* **2**, 782 (2012).
- <sup>148</sup>S. J. Blamires, C. L. Wu, and I. M. Tso, "Variation in protein intake induces variation in spider silk expression," *PLoS One* **7**(2), e31626 (2012).
- <sup>149</sup>E. Steven, W. R. Saleh, V. Lebedev, S. F. A. Acquah, V. Laukhin, R. G. Alamo, and J. S. Brooks, "Carbon nanotubes on a spider silk scaffold," *Nat. Commun.* **4**, 2435 (2013).
- <sup>150</sup>D. Porter, J. Guan, and F. Vollrath, "Spider silk: Super material or thin fibre?," *Adv. Mater.* **25**(9), 1275–1279 (2013).
- <sup>151</sup>M. Marhabaie, T. C. Leeper, and T. A. Blackledge, "Protein composition correlates with the mechanical properties of spider (*Argiope trifasciata*) dragline silk," *Biomacromolecules* **15**(1), 20–29 (2014).
- <sup>152</sup>G. Xu, L. Gong, Z. Yang, and X. Y. Liu, "What makes spider silk fibers so strong? from molecular-crystallite network to hierarchical network structures," *Soft Matter* **10**(13), 2116–2123 (2014).
- <sup>153</sup>S. J. Blamires, C. P. Liao, C. K. Chang, Y. C. Chuang, C. L. Wu, T. A. Blackledge, H. S. Sheu, and I. M. Tso, "Mechanical performance of spider silk is robust to nutrient-mediated changes in protein composition," *Biomacromolecules* **16**(4), 1218–1225 (2015).
- <sup>154</sup>G. B. Perea, C. Solanas, G. R. Plaza, G. V. Guinea, I. Jorge, J. Vázquez, J. M. Pérez Mateos, N. Mari-Buyé, M. Elices, and J. Pérez-Rigueiro, "Unexpected behavior of irradiated spider silk links conformational freedom to mechanical performance," *Soft Matter* **11**(24), 4868–4878 (2015).
- <sup>155</sup>R. Madurga, G. R. Plaza, T. A. Blackledge, G. V. Guinea, M. Elices, and J. Pérez-Rigueiro, "Material properties of evolutionary diverse spider silks described by variation in a single structural parameter," *Sci. Rep.* **6**, 18991 (2016).
- <sup>156</sup>M. Benamú, M. Lacava, L. F. García, M. Santana, J. Fang, X. Wang, and S. J. Blamires, "Nanostructural and mechanical property changes to spider silk as a consequence of insecticide exposure," *Chemosphere* **181**, 241–249 (2017).
- <sup>157</sup>E. Lepore, F. Bosia, F. Bonaccorso, M. Bruna, S. Taiolo, G. Garberoglio, A. Ferrari, and N. M. Pugno, "Silk reinforced by graphene or carbon nanotubes," *2D Mater.* **4**, 031013 (2017).
- <sup>158</sup>S. R. Koebley, F. Vollrath, and H. C. Schniepp, "Toughness-enhancing meta-structure in the recluse spider's looped ribbon silk," *Mater. Horiz.* **4**(3), 377–382 (2017).
- <sup>159</sup>J. Xu, Q. Dong, Y. Yu, B. Niu, D. Ji, M. Li, Y. Huang, X. Chen, and A. Tan, "Mass spider silk production through targeted gene replacement in *Bombyx mori*," *Proc. Natl. Acad. Sci. U. S. A.* **115**(35), 8757–8762 (2018).
- <sup>160</sup>G. G. Kerr, H. F. Nahrung, A. Wiegand, J. Kristoffersen, P. Killen, C. Brown, and J. Macdonald, "Mechanical properties of silk of the Australian golden orb weavers *Nephila pilipes* and *Nephila plumipes*," *Biol. Open* **7**(2), bio029249 (2018).
- <sup>161</sup>D. Piorowski, S. J. Blamires, N. E. Doran, C. P. Liao, C. L. Wu, and I. M. Tso, "Ontogenetic shift toward stronger, tougher silk of a web-building, cave-dwelling spider," *J. Zool.* **304**, 81–89 (2017).
- <sup>162</sup>S. J. Blamires, M. Nobbs, P. J. Martens, I. M. Tso, W. T. Chuang, C. K. Chang, and H. S. Sheu, "Multiscale mechanisms of nutritionally induced property variation in spider silks," *PLoS One* **13**(2), e0192005 (2018).
- <sup>163</sup>K. Yazawa, A. D. Malay, H. Masunaga, and K. Numata, "Role of skin layers on mechanical properties and supercontraction of spider dragline silk fiber," *Macromol. Biosci.* **19**(3), 1800220 (2019).
- <sup>164</sup>C. Viera, L. F. Garcia, M. Lacava, J. Fang, X. Wang, M. M. Kasumovic, and S. J. Blamires, "Silk physico-chemical variability and mechanical robustness facilitates intercontinental invasibility of a spider," *Sci. Rep.* **9**(1), 13273 (2019).
- <sup>165</sup>J. Garrote, V. Ruiz, O. P. Troncoso, F. G. Torres, M. Arnedo, M. Elices, G. V. Guinea, and J. Pérez-Rigueiro, "Application of the spider silk standardization initiative (S3I) methodology to the characterization of major ampullate gland silk fibers spun by spiders from Pantanos de Villa Wetlands (Lima, Peru)," *J. Mech. Behav. Biomed. Mater.* **111**, 104023 (2020).
- <sup>166</sup>R. W. Work and P. D. Emerson, "An apparatus and technique for the forcible silking of spiders," *J. Arachnol.* **10**(1), 1–10 (1982).
- <sup>167</sup>M. F. Pantano, R. Tatti, L. Aversa, R. Verucchi, and N. M. Pugno, "Doubling the mechanical properties of spider silk by c60 supersonic molecular beam epitaxy," *Front. Mater.* **7**, 197 (2020).
- <sup>168</sup>H.-C. Wu, A. Pandey, L.-Y. Chang, C.-Y. Hsu, T. C.-K. Yang, I.-M. Tso, H.-S. Sheu, and J.-C. Yang, "Hydrothermal effect on mechanical properties of *Nephila pilipes*," *Polymers* **12**(1013), 1013 (2020).
- <sup>169</sup>S. P. Kelly, K. P. Huang, C. P. Liao, R. A. N. Khasanah, F. S. S. Chien, J. S. Hu, C. L. Wu, and I. M. Tso, "Mechanical and structural properties of major ampullate silk from spiders fed carbon nanomaterials," *PLoS One* **15**, e0241829 (2020).
- <sup>170</sup>G. Greco and N. M. Pugno, "Mechanical properties and Weibull scaling laws of unknown spider silks," *Molecules* **25**, 2938 (2020).
- <sup>171</sup>G. Greco, J. Wolff, and N. M. Pugno, "Strong and tough silk for resilient attachment discs: The mechanical properties of piriform silk, in the spider *Cupiennius salei* (Keyserling, 1877)," *Front. Mater.* **7**, 138 (2020).

- <sup>172</sup>L. Hu, Q. Chen, J. Yao, Z. Shao, and X. Chen, "Structural changes in spider dragline silk after repeated supercontraction—stretching processes," *Biomacromolecules* **12**, 5306 (2020).
- <sup>173</sup>T. W. Dugger, S. Sarkar, S. M. Correa-Garhwal, M. Zhernenkov, Y. Zhang, G. Kolhatkar, R. Mohan, L. Cruz, A. D. Lubio, A. Ruediger, C. Y. Hayashi, K. E. Urich, and D. J. Kisailus, "Ultrastructures and mechanics of annealed *Nephila clavipes* major ampullate silk," *Biomacromolecules* **21**(3), 1186–1194 (2020).
- <sup>174</sup>M. Saric, L. Eisoldt, V. Döring, and T. Scheibel, "Interplay of different major ampullate spidroins during assembly and implications for fiber mechanics," *Adv. Mater.* **33**(9), 2006499 (2021).
- <sup>175</sup>D. Piorkowski, C. P. Liao, T. A. Blackledge, and I. M. Tso, "Size-related increase in inducible mechanical variability of major ampullate silk in a huntsman spider (Araneae: Sparassidae)," *Sci. Nat.* **108**(3), 22 (2021).
- <sup>176</sup>K. Yazawa, K. Hidaka, and J. Negishi, "Cell adhesion behaviors on spider silk fibers, films, and nano fibers," *Langmuir* **38**, 7766 (2022).
- <sup>177</sup>A. E. Brooks, S. M. Stricker, S. B. Joshi, T. J. Kamerzell, C. R. Middaugh, and R. V. Lewis, "Properties of synthetic spider silk fibers based on *Argiope aurantia* MaSp2," *Biomacromolecules* **9**(6), 1506–1510 (2008).
- <sup>178</sup>Z. Lin, Q. Deng, X. Y. Liu, and D. Yang, "Engineered large spider eggcase silk protein for strong artificial fibers," *Adv. Mater.* **25**(8), 1216–1220 (2012).
- <sup>179</sup>A. E. Albertson, F. Teulé, W. Weber, J. L. Yarger, and R. V. Lewis, "Effects of different post-spin stretching conditions on the mechanical properties of synthetic spider silk fibers," *J. Mech. Behav. Biomed. Mater.* **29**, 225–234 (2014).
- <sup>180</sup>C. G. Copeland, B. E. Bell, C. D. Christensen, and R. V. Lewis, "Development of a process for the spinning of synthetic spider silk," *ACS Biomater. Sci. Eng.* **1**(7), 577–584 (2015).
- <sup>181</sup>M. Andersson, Q. Jia, A. Abella, X. Y. Lee, M. Landreh, P. Purhonen, H. Hebert, M. Tenje, C. V. Robinson, Q. Meng, G. R. Plaza, J. Johansson, and A. Rising, "Biomimetic spinning of artificial spider silk from a chimeric minispidroin," *Nat. Chem. Biol.* **13**(3), 262–264 (2017).
- <sup>182</sup>R. Madurga, A. M. Gañán-Calvo, G. R. Plaza, G. V. Guinea, M. Elices, and J. Pérez-Rigueiro, "Production of high performance bioinspired silk fibers by straining flow spinning," *Biomacromolecules* **18**(4), 1127–1133 (2017).
- <sup>183</sup>C. Thamm and T. Scheibel, "Recombinant production, characterization, and fiber spinning of an engineered short major ampullate spidroin (MaSp1s)," *Biomacromolecules* **18**(4), 1365–1372 (2017).
- <sup>184</sup>R. Madurga, A. M. Gañán-Calvo, G. R. Plaza, J. M. Atienza, G. V. Guinea, M. Elices, P. A. López, R. Daza, D. González-Nieto, and J. Pérez-Rigueiro, "Comparison of the effects of post-spinning drawing and wet stretching on regenerated silk fibers produced through straining flow spinning," *Polymers* **10**, 311–317 (2018).
- <sup>185</sup>L. Xu, N. Weatherbee-Martin, X. Q. Liu, and J. K. Rainey, "Recombinant silk fiber properties correlate to prefibrillar self-assembly," *Small* **15**(12), 1805294 (2019).
- <sup>186</sup>Y. Yuan, Q. Yu, J. Wen, C. Li, Z. Guo, X. Wang, and N. Wang, "Ultrafast and highly selective uranium extraction from seawater by hydrogel-like spidroin-based protein fiber," *Angew. Chem.* **131**(34), 11911–11916 (2019).
- <sup>187</sup>R. Wen, K. Wang, and Q. Meng, "Characterization of the second type of aciniform spidroin (AcSp2) provides new insight into design for spidroin-based biomaterials," *Acta Biomater.* **115**, 210–219 (2020).
- <sup>188</sup>C. Zhang, J. Mi, H. Qi, J. Huang, S. Liu, L. Zhang, and D. Fan, "Engineered a novel pH-sensitive short major ampullate spidroin," *Int. J. Biol. Macromol.* **154**, 698–705 (2020).
- <sup>189</sup>L. Y. Tian, Q. Meng, and Y. Lin, "Expression and characterization of chimeric spidroins from flagelliform-aciniform repetitive modules," *Biopolymers* **111**(12), e23404 (2020).
- <sup>190</sup>H. Zhu, A. Rising, J. Johansson, X. Zhang, Y. Lin, L. Zhang, T. Yi, J. Mi, and Q. Meng, "Tensile properties of synthetic pyriform spider silk fibers depend on the number of repetitive units as well as the presence of N- and C-terminal domains," *Int. J. Biol. Macromol.* **154**, 765–772 (2020).
- <sup>191</sup>X. Li, X. Qi, Y. M. Cai, Y. Sun, R. Wen, R. Zhang, J. Johansson, Q. Meng, and G. Chen, "Customized flagelliform spidroins form spider silk-like fibers at pH 8.0 with outstanding tensile strength," *ACS Biomater. Sci. Eng.* **8**(1), 119–127 (2022).
- <sup>192</sup>T. Asakura, H. Matsuda, A. Aoki, and A. Naito, "Acetylation and hydration treatment of recombinant spider silk fiber, and their characterization using <sup>13</sup>C NMR spectroscopy," *Polymers* **243**, 124605 (2022).
- <sup>193</sup>Q. Jin, F. Pan, C. F. Hu, S. Y. Lee, X. X. Xia, and Z. G. Qian, "Secretory Production of spider silk proteins in metabolically engineered *Corynebacterium glutamicum* for spinning into tough fibers," *Metab. Eng.* **70**, 102–114 (2022).
- <sup>194</sup>W. He, D. Qian, Y. Wang, G. Zhang, Y. Cheng, X. Hu, K. Wen, M. Wang, Z. Liu, X. Zhou, and M. Zhu, "Protein-like nanogel for spinning hierarchically structured artificial spider silk," *Adv. Mater.* **34**, 2201843 (2022).
- <sup>195</sup>T. Asakura, H. Matsuda, A. Naito, and Y. Abe, "Formylation of recombinant spider silk in formic acid and wet spinning studied using nuclear magnetic resonance and infrared spectroscopies," *ACS Biomater. Sci. Eng.* **8**, 2390 (2022).
- <sup>196</sup>J. Cheng, C. Hu, C. Gan, X. Xia, and Z. Qian, "Functionalization and reinforcement of recombinant spider dragline silk fibers by confined nanoparticle formation," *ACS Biomater. Sci. Eng.* **8**, 3299 (2022).



1 **Supplementary Material:**

2 **Influence of experimental methods on the mechanical properties of silk fibers: A**  
3 **systematic literature review and future road map**

4  
5 Gabriele Greco <sup>a,b\*</sup>, Benjamin Schmuck<sup>a,c</sup>, S.K. Jalali<sup>b</sup>, Nicola M. Pugno<sup>b,d</sup> and Anna  
6 Rising<sup>a,c\*</sup>

7 *<sup>a</sup> Department of Anatomy, Physiology and Biochemistry, Swedish University of Agricultural*  
8 *Sciences, Uppsala, Sweden*

9 *<sup>b</sup> Laboratory for Bioinspired, Bionic, Nano, Meta, Materials & Mechanics, Department of*  
10 *Civil, Environmental and Mechanical Engineering, University of Trento, Via Mesiano, 77,*  
11 *38123 Trento, Italy*

12 *<sup>c</sup> Department of Biosciences and Nutrition, Karolinska Institutet, Neo, 141 86 Huddinge,*  
13 *Sweden*

14 *<sup>d</sup>School of Engineering and Materials Science, Queen Mary University of London, Mile End*  
15 *Road, London E1 4NS, UK*

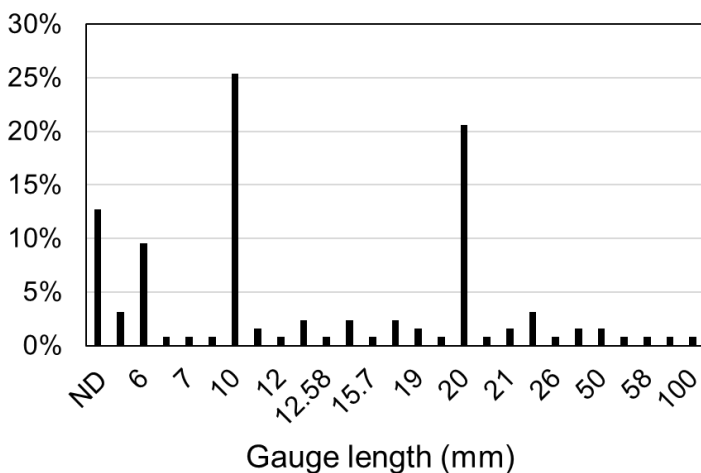
16 \* Corresponding author: [gabriele.greco@slu.se](mailto:gabriele.greco@slu.se); [anna.rising@ki.se](mailto:anna.rising@ki.se);

17

18 Supplementary section 1 (S1): why we do not consider here the gauge length

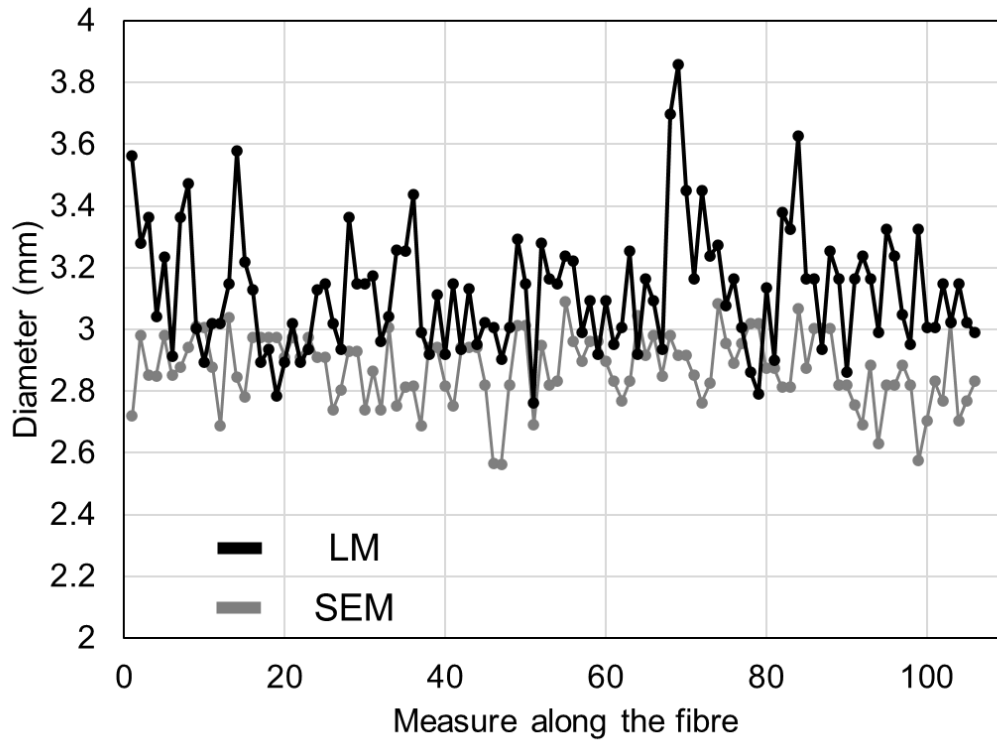
19 The sample dimension (i.e., fiber length, gauge length) is a further element to take into  
20 account when comparing the mechanical properties of different fibers. In principle, the  
21 occurrence of defects is positively correlated to fiber length<sup>200-202</sup>, hence shorter gauge  
22 lengths will result in higher strength compared to longer ones. Different gauge lengths are  
23 used in the silk field, and 12.5% of the studies herein considered (Table 1) did not even  
24 mention them (Figure S1). On the other hand, the majority of the studies in the silk field use  
25 gauge lengths between 5-20 mm, which do not give large differences<sup>57,73,125,172</sup>. For this  
26 reason, fiber length will not be further discussed here.

27



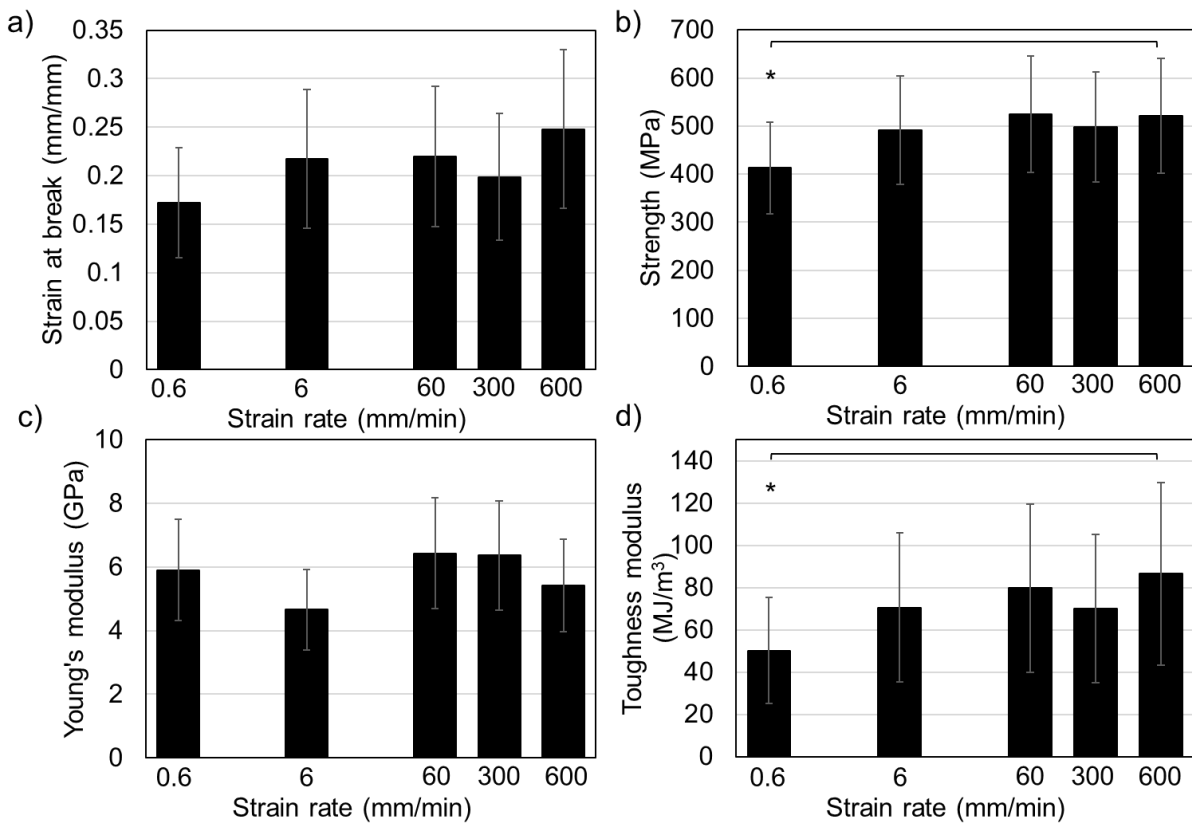
28

29 *Figure S1: Gauge length values of the fibers tested mechanically in literature. Percentages calculated based on Table 1.*



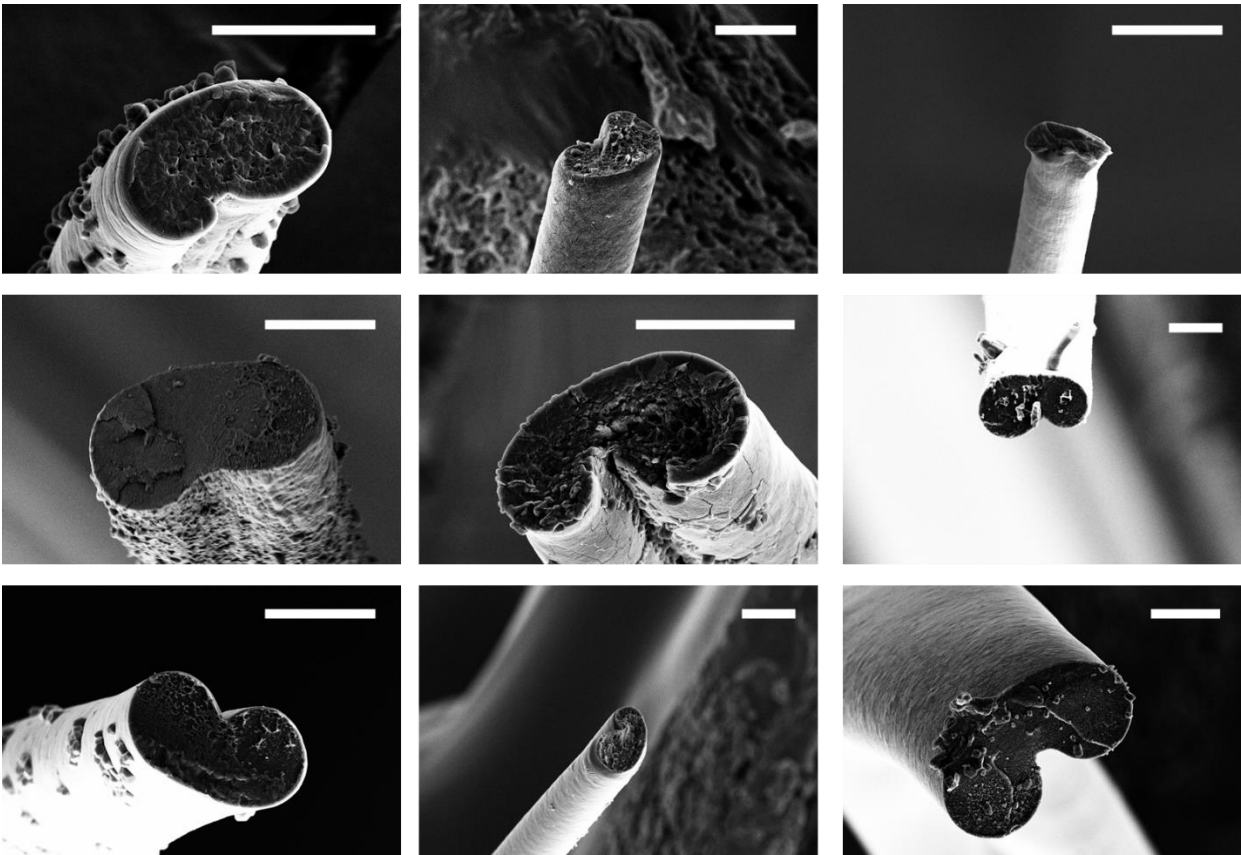
30

31 *Figure S2: Diameters values measured along the same fibers first with LM and then with SEM, which constantly displays*  
 32 *lower values.*



33

34 *Figure S3: Mechanical properties of Bombyx mori silk fibers measured at different strain rates. a) Strain at break, b)*  
 35 *strength, c) Young's modulus, and d) toughness modulus. Stars indicate that the difference is significant (p-value*  
 36 *<0.05). The error bars are standard deviations.*



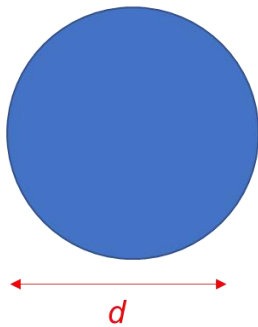
37

38 *Figure S4: Representative SEM images of the cross-sections of the NT2RepCT fibers, in which is possible to observe*  
 39 *the non-circular cross-section. Scale bars are 10 μm.*

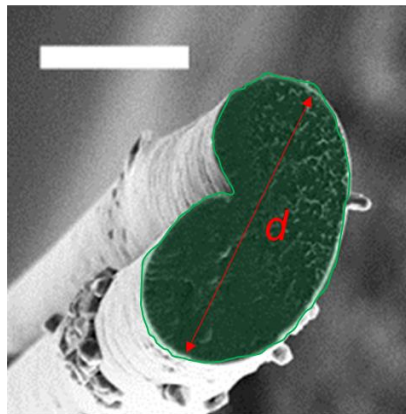
40

41

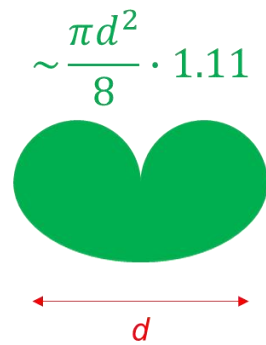
a) Assumed Geometry



b)



c) Real Geometry



d)

$$\frac{\frac{\pi d^2}{4}}{\frac{\pi d^2}{8} \cdot 1.11} \sim 1.80$$

e)

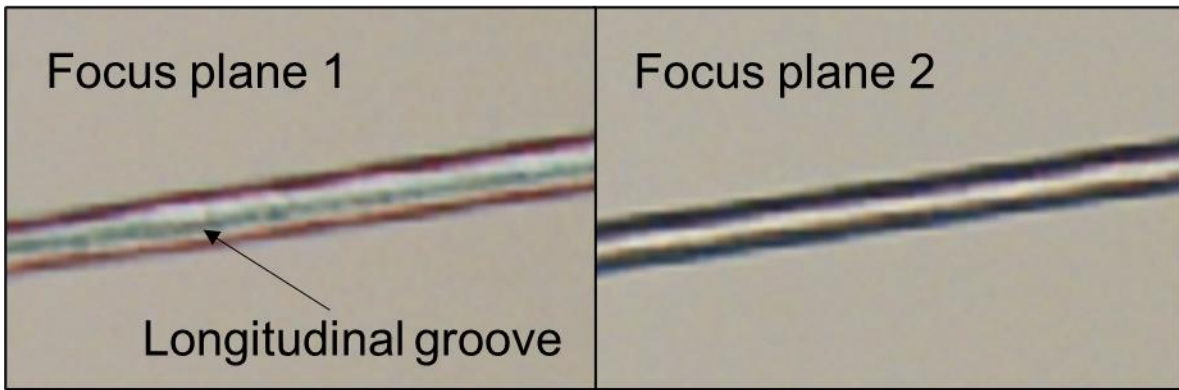
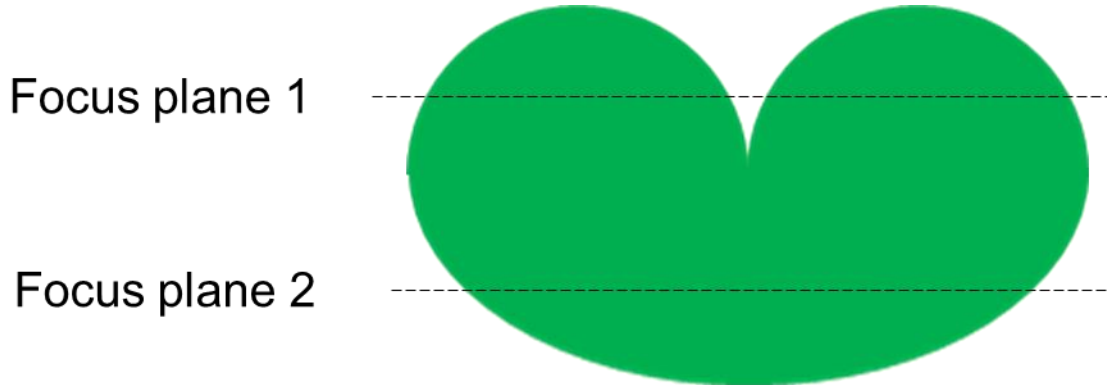
From the measurements:

$$1.81 \pm 0.31$$

42

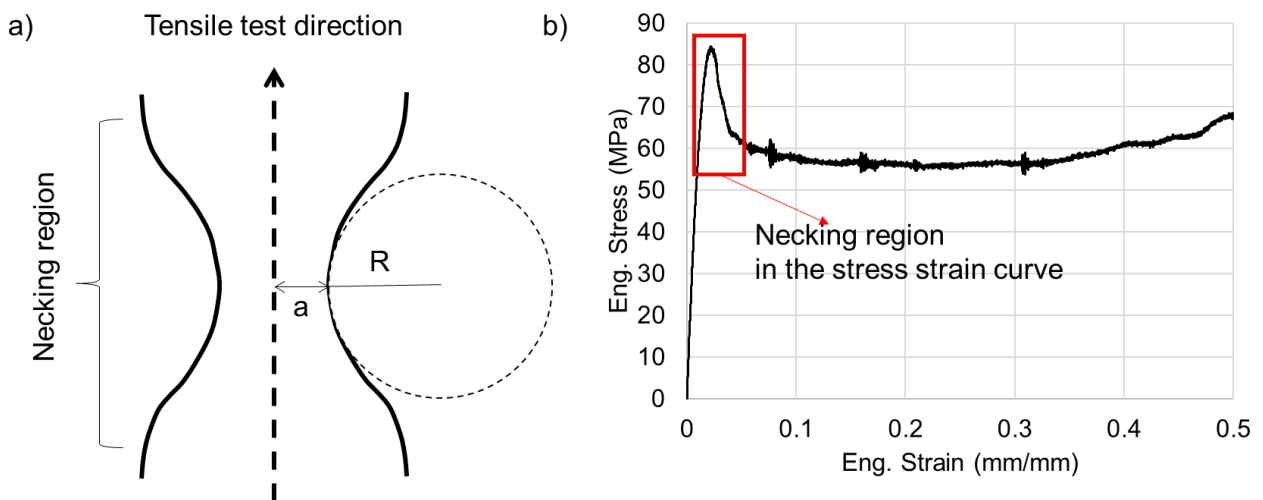
43 *Figure S5: a) Measurement of the “diameter” and the cross-sectional area are usually performed assuming the fibers as*  
 44 *circular in cross section. b) Many artificial silk fibers are not circular in cross section, as shown here for a NT2RepCT*

45 fiber. The fibers' diameter is usually measured as depicted in red. c) A simple geometrical model showing how the true  
 46 cross-sectional area of a fiber with the morphology shown in c) could be calculated, d) the ratio between the area of the  
 47 circle and the real cross section assuming same "diameter", e) and the measured values of this ratio (coming from 100  
 48 measurements).

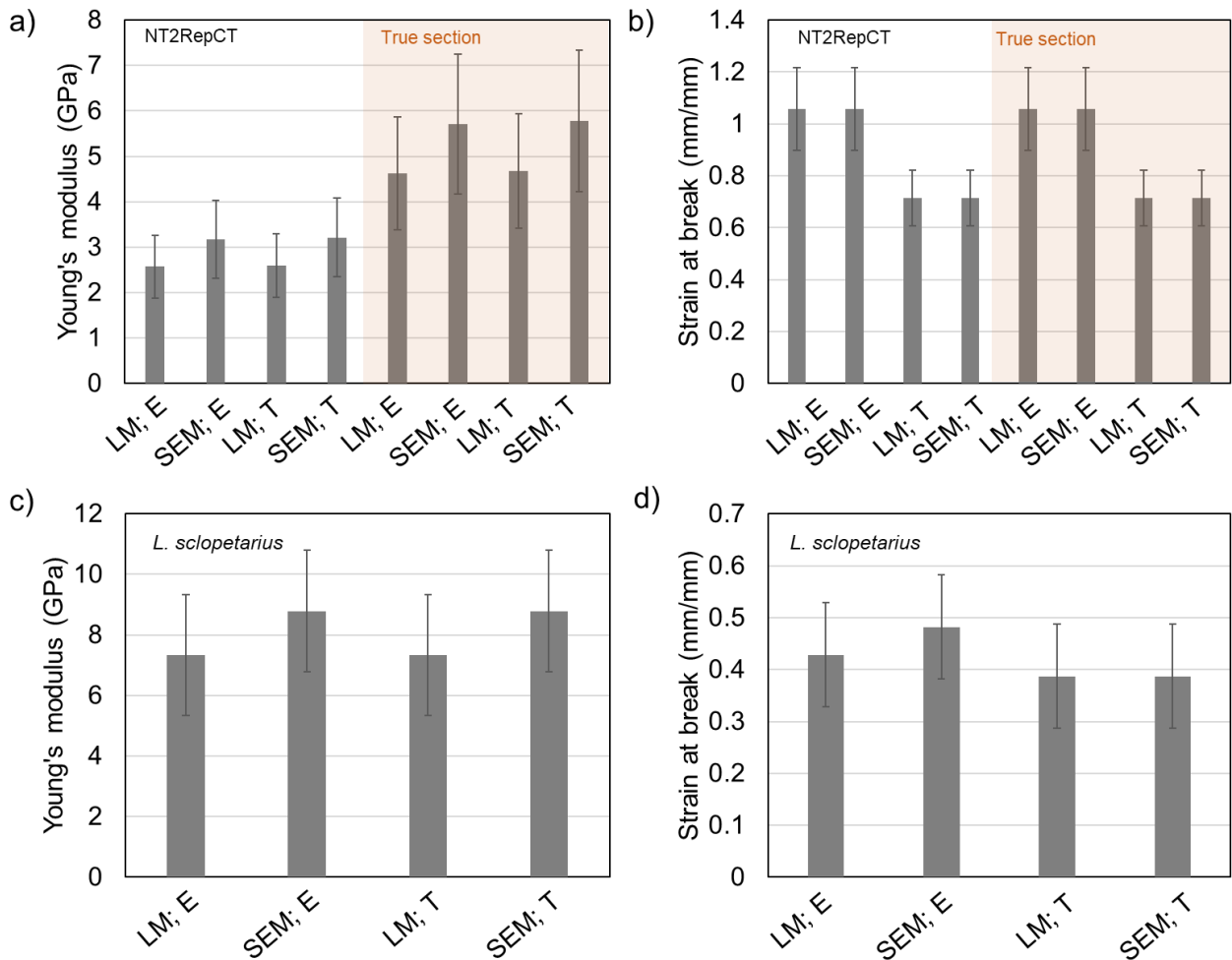


49  
 50 Figure S6: Some specific details of the fibers (e.g., longitudinal groove) may be not easily detectable by using Light  
 51 Microscopy, where a slight change in Z position (focus) could impede the correct evaluation of a feature.

52  
 53



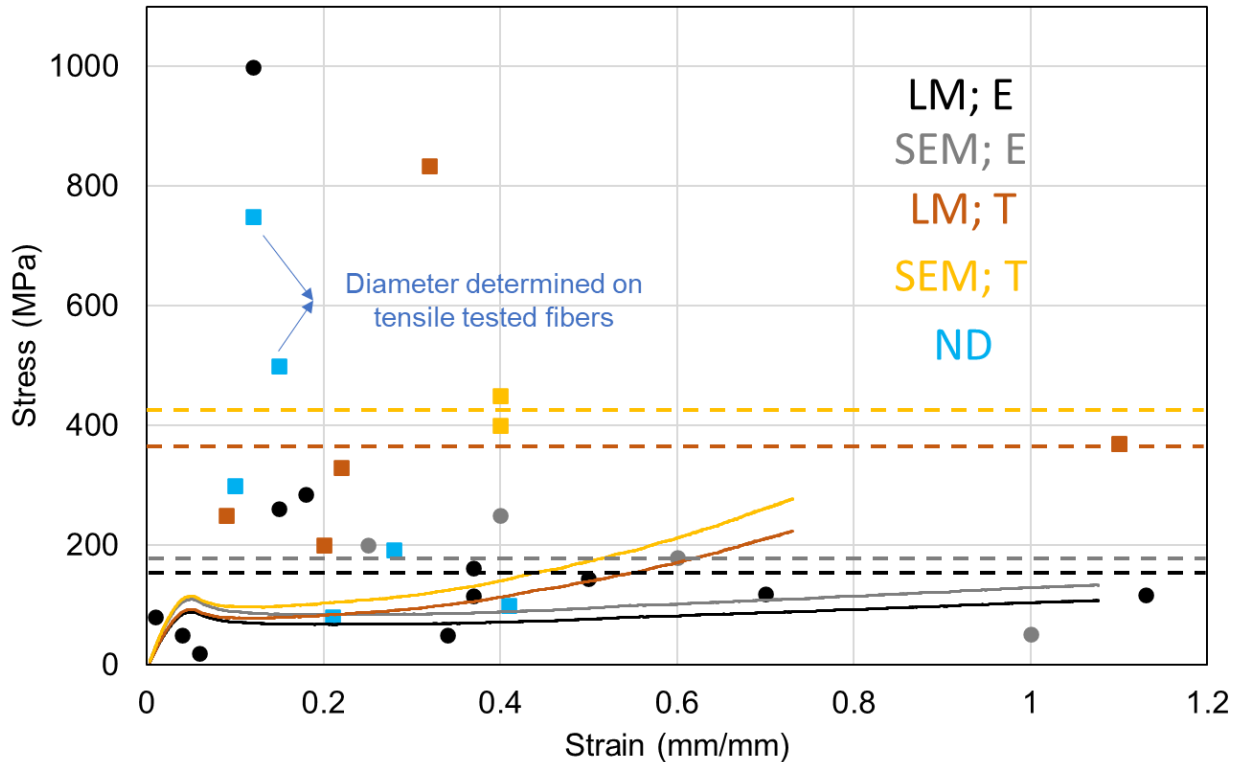
54  
 55 Figure S7: a) Schematic of the necking region, with the reduced radius "a" and the instant radius of curvature R. b)  
 56 Necking phenomenon observed in the stress strain curve.



57

58 Figure S8: a) Young's modulus and b) strain at break of the same set of NT2RepCT fibers calculated with different  
 59 accepted methods. c) young's modulus and d) strain at break of the same set of *L. scolopetarius* fibers calculated with  
 60 different method compared with the values taken from literature with similar methods. LM = diameter measured with  
 61 Light Microscopy; E = Engineering stress and strain; SEM = diameter measured with Scanning Electron Microscopy; T =  
 62 True stress and true strain calculation. The error bars are standard deviations.



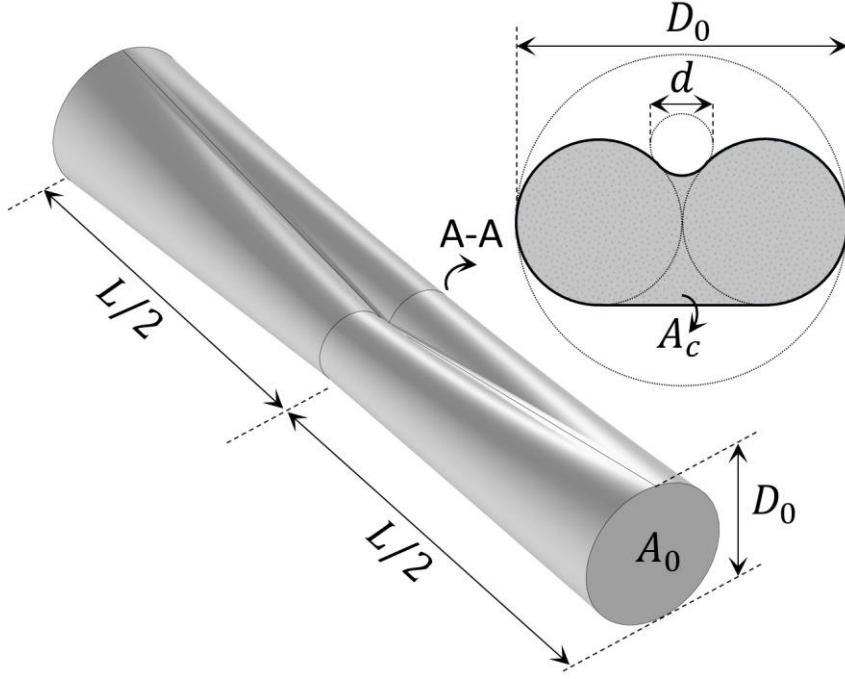


63

64 Figure S9: Stress strain curves of a representative NT2RepCT fibers obtained by using Engineering stress and strain (E)  
 65 or True stress and strain (T), and by measuring the diameter with Scanning Electron Microscopy (SEM) or Light  
 66 Microscopy (LM). In the same graph, the single stress and strain at break points of artificial silk fibers taken from  
 67 literature (averages) are reported. ND means that the choice of method under which the mechanical properties were  
 68 obtained was not declared. Literature data were obtained from<sup>30,32,104–106,156,177,180–184,96,185–187,189–193,195,196,97,203,204,98–103</sup>.  
 69 The dashed lines indicate the average of all the vales of strength found in the literature. The error bars are standard  
 70 deviations.

71 Supplementary section 2 (S2): Stress concentration factor for imperfected spider silk

72 In this section, the stress concentration raised from the observed imperfection in the artificially  
 73 manufactured spider silk is evaluated implementing finite element analysis. The schematic of the  
 74 geometric model is illustrated in Fig. 1. Consider a spider silk fiber of the nominal diameter of  $D_0$  and  
 75 the nominal cross section area of  $A_0 = \pi D_0^2/4$ , whose cross section is affected by a longitudinal  
 76 imperfection along a total length of  $L$  resulting in a symmetrical tapering. The cross section is  
 77 continuously reduced from  $A_0$  to a minimum area,  $A_c$ , at the center of imperfection by lofting, see  
 78 section A-A in Fig. 1. To regulate the sharpness of the groove along the fiber, a filet of diameter  $d$  is  
 79 introduced.



80

81 **Fig. 1:** The schematic of the geometric model of the longitudinal imperfection in the artificial spider  
82 silk.

83

84 One can obtain the ratio of the minimum cross section area at the center,  $A_c$ , to the nominal area,  
85  $A_0$ , as a function of dimensionless ratio,  $d/D_0$ , as:

$$\frac{A_c}{A_0} = \frac{1}{2} \left( \frac{1}{\pi} + \frac{3}{4} \right) + \frac{1}{2\pi} \sqrt{(d/D_0)^2 + (d/D_0)} - \frac{1}{4} \left( \frac{1}{2} + \frac{\theta}{\pi} \right) - \frac{\theta}{\pi} (d/D_0)^2 \quad (1a)$$

86 were

$$\theta = \sin^{-1} \left( \frac{1}{1 + 2(d/D_0)} \right) \quad (1b)$$

87 this area ratio,  $A_c/A_0$ , varies slightly with respect to  $d/D_0$  from a minimum of  $\frac{(3\pi/4+1)}{2\pi} \approx 0.534$  to a  
88 maximum of  $\frac{(\pi/4+1)}{\pi} \approx 0.568$ , corresponding to  $d = 0$  (sharp groove), and  $d = \infty$  (no groove),  
89 respectively.

90 According to the equilibrium along the axis of the fiber, the average stress at the central cross  
91 section,  $\sigma_{ave}$ , is related to the applied axial stress on the nominal cross section out of the imperfed  
92 length,  $\sigma_0$ :

$$\sigma_{ave} = \frac{\sigma_0}{(A_c/A_0)} \quad (2a)$$

93 However, the actual distribution of the axial stress on the central cross section is not uniform as a  
94 result of tapering, oval, and existence of the groove. The maximum stress in the central section is  
95 related to the average one by introducing the stress concentration factor,  $K$ , as (see Fig. 2) [1]:

$$\sigma_{max} = K \sigma_{ave} \quad (2b)$$

96 The maximum stress can be related to the nominal applied stress by combining Eqs. (2a) and (2b):

$$\sigma_{max} = \frac{K \sigma_0}{(A_c/A_0)} \quad (2c)$$

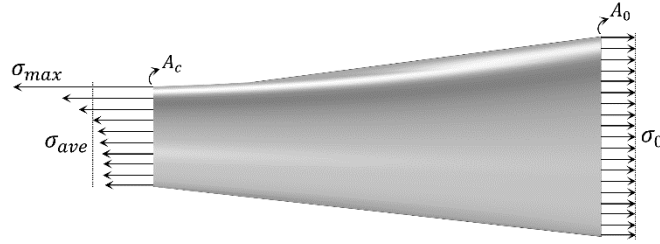


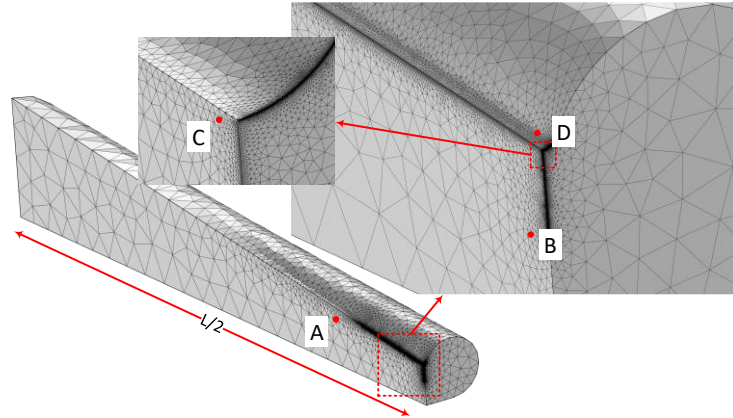
**Fig. 2:** Definition of stresses in the model.

97  
98  
99

100 A set of numerical simulations based on finite element analysis using COMSOL Multiphysics®  
101 software is performed to find the stress concentration factor,  $K$ , as a function of geometric  
102 parameters of the imperfection. Considering the symmetry, a quarter of the geometry is discretized  
103 by the quadratic mesh type. An extra fine meshing in the zone of stress concentration is considered  
104 by manually controlling the number of nodes,  $n$ , along every sensitive edge, i.e., CA, CB, and CD,  
105 as shown in Fig. 3. A sample convergence study for validating mesh independency of results is  
106 presented in Fig. 4. It is observed that for  $n = 500$  the results show acceptable converged, therefore,  
107 this value is used for all the simulations. A linear elastic material is defined and the effect of Poisson's  
108 ratio on the stress concentration factor,  $K$ , is investigated by varying it in a wide range of  $-1 < \nu <$   
109  $0.5$ . The Young's modulus is set to 2.6 GPa corresponding to the measured value for the artificial  
110 silk fiber, however, it is noted that the obtained stress concentration factor from the linear analysis is  
111 not sensitive to the value of young's modulus. A uniform axial stress is applied on the reference area,  
112  $A_0$ , and the stress concentration factor is extracted by dividing the maximum to the average stress  
113 on the minimum area,  $A_c$ , at the center of imperfection. A sample of stress contours are presented  
114 in Fig. 5 which clearly reveals the existence of a stress concentration with a maximum at the centre  
115 of the longitudinal groove.

116 Fig. 6 plots the stress concentration factor with respect to the dimensionless tapering length,  $L/D_0$ ,  
117 for different dimensionless sharpness of longitudinal groove,  $d/D_0$ . It is observed that tapering length  
118 has the main impact on the stress concentration. For relatively short imperfections,  $L/D_0 < 4$ , even  
119 for the case of almost removed groove with  $d/D_0 = 6$ , the stress concentration is higher than three,  
120  $K > 3$ , however, by increasing the tapering length, the stress concentration dramatically decreases  
121 and it is seen that for  $L/D_0 > 13$ , even for a sharp groove with  $d/D_0 = 0.05$  the stress concentration  
122 factor is less than two,  $K < 2$ . In general, it is concluded that the observed unfavorable longitudinal  
123 imperfection in the artificial silk fibers causes an unignorable stress concentration that will  
124 significantly affect the tensile properties of the fibers. Since the artificial silk is not brittle, this stress  
125 concentration results in a local yielding forming a plastic zone which grows by increasing the applied  
126 load which alerts the stress-strain curves obtained from tensile tests on these fibers. Besides, it is  
127 revealed that decreasing the Poisson's ratio from  $\nu = 0.3$  to  $\nu = 0.1$  slightly decreases the stress  
128 concentration. Fig. 7 focuses on the effect of Poisson's ratio on the stress concentration factor. To  
129 demonstrate the influence of geometry a long-grooved length with  $L/D_0 = 18$  and a very short groove  
130 with  $L/D_0 = 2$  is considered and for every groove two different sharpness, i.e.,  $d/D_0 = 0.05$  and  $0.2$   
131 are assumed. The Poisson's ratio has changed in the range of  $-0.95$  to  $0.49$  since the exact bonds  
132 of  $\nu = -1$  and  $0.5$  are not accessible in the numerical simulations. Results from finite element  
133 simulations reveal that approaching both upper and lower limits of Poisson's ratio increase the stress  
134 concentration especially when  $\nu \rightarrow -1$ . It provides a specific Poisson's ratio that minimizes the stress  
135 concentration factor according to the geometrical parameters of the longitudinal imperfection, i.e.,  
136  $L/D_0$ , and  $d/D_0$ , which is presented in Fig. 7. One can observe that for a certain groove length,  
137 increasing the sharpness, shifts  $\nu_{opt}$  to the left while decreasing the groove length results in a shift  
138 to the right.

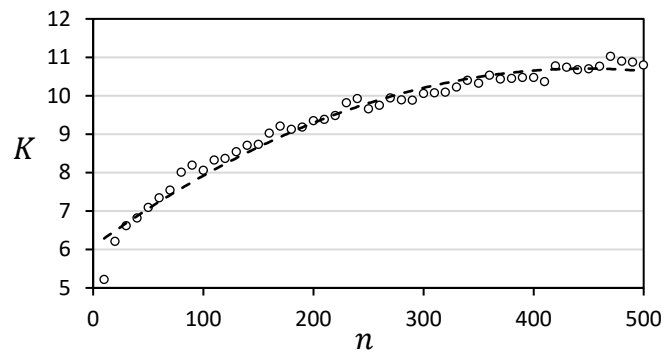
139



140

141

**Fig. 3:** Discretization of a quarter of the model with extra fine meshing in the vicinity of high stress concentration zone.

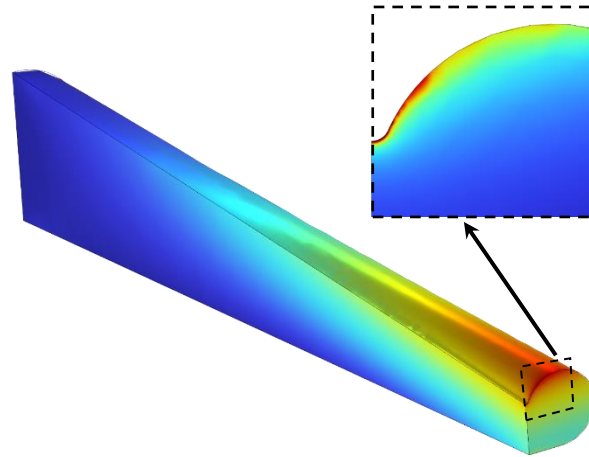


142

143

144

**Fig. 4:** Convergence study on mesh dependency of the finite element results.

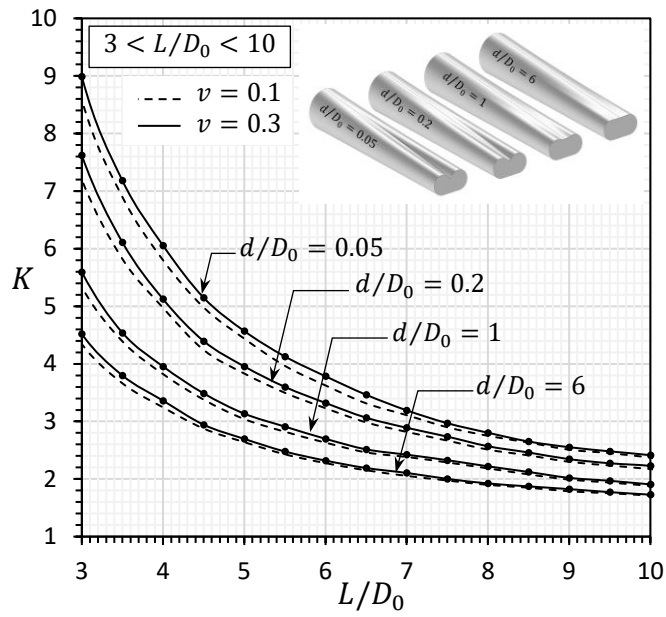


145

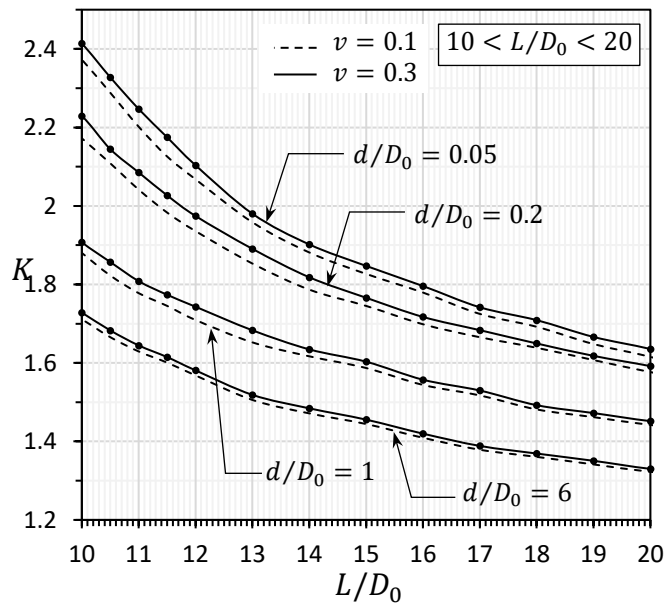
146

147

**Fig. 5:** A sample contour for von Mises stress of the grooved artificial spider silk fiber.



148



149

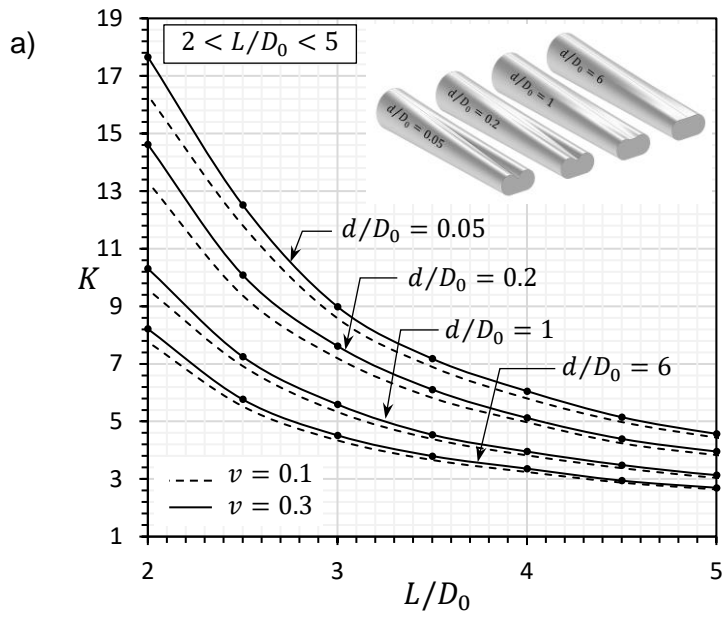
150

151

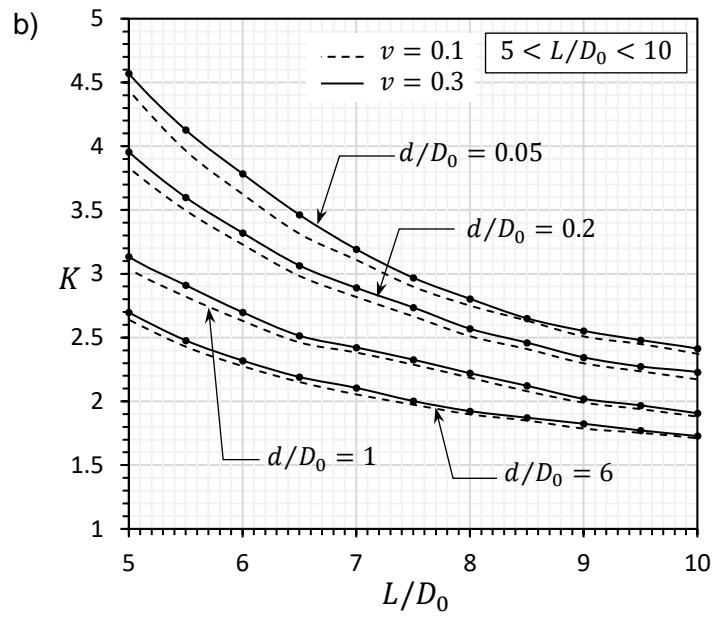
152

153

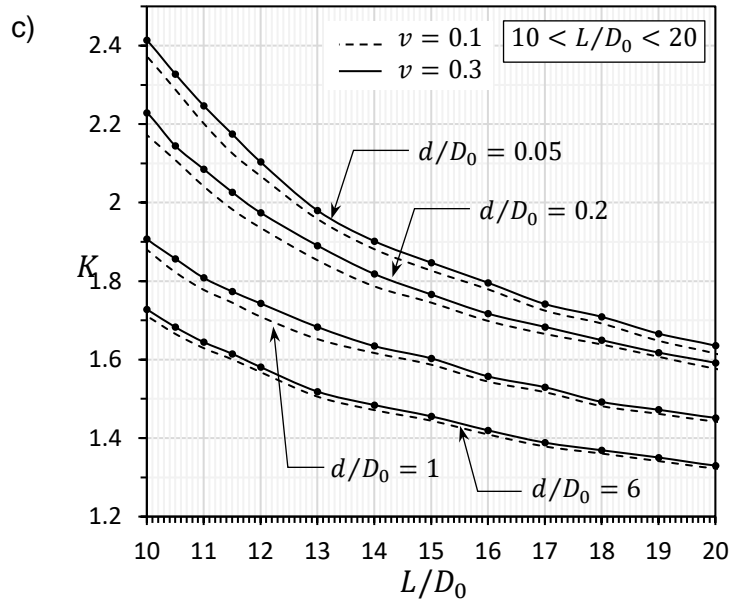
**Fig. 6:** Stress concentration factor,  $K$ , versus the dimensionless grooved length,  $L/D_0$ , for different sharpness of the longitudinal groove,  $d/D_0$  obtained from finite element analysis.



154

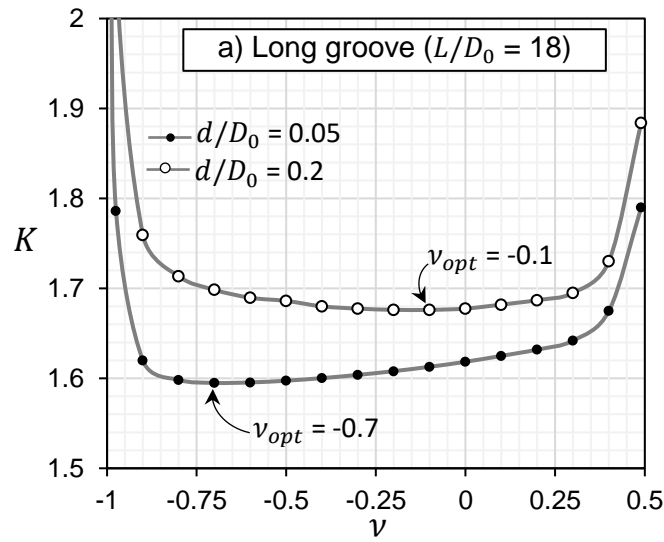


155

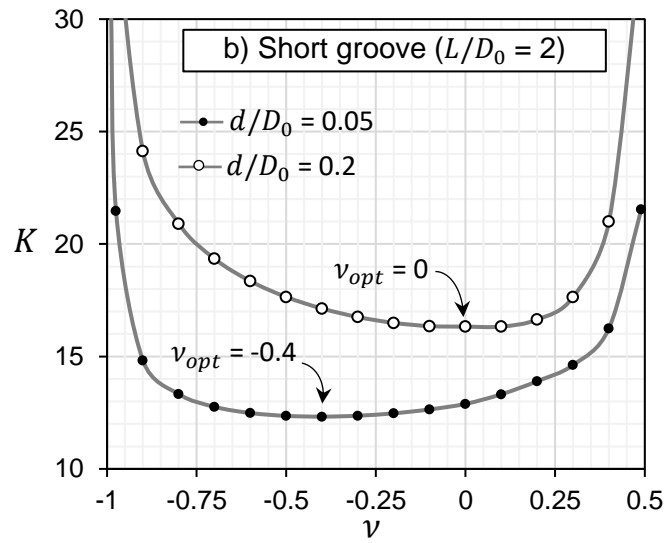


156  
157  
158

**Fig. 6:** Stress concentration factor,  $K$ , versus the dimensionless grooved length,  $L/D_0$ , for different sharpness of the longitudinal groove,  $d/D_0$  obtained from finite element analysis a), b), and c).



159



160



161 **Fig. 7:** The effect of Poisson's ratio on the Stress concentration factor,  $K$ , for different dimensionless groove length,  
 162  $L/D_0=18$  and  $2$  and for different dimensionless sharpness of the longitudinal groove,  $d/D_0=0.05$  and  $0.2$  obtained from  
 163 finite element analysis.

164  
 165

166 Supplementary section 3 (S3): Calculation of true stress and strain

167 Equations 1 and 2 are not valid if the cross section  $A_0$  and the gauge length  $L_0$  continuously vary  
 168 with the increase of the deformation. Thus, one might consider the instantaneous cross section  $A$   
 169 and length  $L$ . In this context, the instantaneous increase in deformation during the tensile test can  
 170 be expressed as

171 
$$d\epsilon = \frac{dL}{L}$$

172 By integrating this expression between  $L_0$  and  $L$  the true strain expression is correctly obtained as  
 173 depicted in equation (4)

174 
$$\epsilon_T = \ln(1 + \epsilon)$$

175

176 Equation (3), on the other hand can be obtained in two different ways. In the first one, the constancy  
 177 of the volume is assumed as in Guinea et al.<sup>116</sup>. This means that at every instant

178 
$$A_0 L_0 = AL$$

179 from which it is possible to calculate the true stress as

180 
$$\sigma_T = \frac{F}{A} = \frac{FL}{A_0 L_0} = \sigma(1 + \epsilon)$$

181 The exact way to calculate the true stress considers the deformation ruled by the Poisson's  
 182 effect. In particular the instantaneous area  $A$  could be calculated as

183 
$$A = a(1 - \nu\epsilon)b(1 - \nu\epsilon) = ab(1 - \nu\epsilon)^2 = A_0(1 - \nu\epsilon)^2$$

184 where  $a$  and  $b$  are the two cross-sectional dimensions. For circular fibers

185 
$$A_0 = \frac{\pi D_0^2}{4}$$

186 where  $D_0$  is the diameter of the fiber. Thus:

187 
$$\sigma_T = \frac{F}{A_0(1 - \nu\epsilon)^2} = \frac{\sigma}{(1 - \nu\epsilon)^2} \quad (5)$$

188 This expression can be expanded in Taylor's series for moderate strain  $\epsilon$  as

189 
$$\sigma_T \sim \sigma(1 + 2\nu\epsilon)$$

190 which is equation 3 only if  $\nu=1/2$ . This second way of deriving the true stress remarks the  
 191 fact that the expression 3 used by the silk community is only valid for moderate deformations  
 192 and  $\nu=1/2$ , which is not the case for many silk-based materials, and thus must be substituted  
 193 with equation 5.

194